REVIEWS OF GEOPHYSICS AND SPACE PHYSICS, VOL. 20, NO. 1, PAGES 67–89, FEBRUARY 1982

Optical Properties of Snow

STEPHEN G. WARREN[1]

Cooperative Institute for Research in Environmental Sciences, University of Colorado
Boulder, Colorado 80309

Measurements of the dependence of snow albedo on wavelength, zenith angle, grain size, impurity content, and cloud cover can be interpreted in terms of single-scattering and multiple-scattering radiative transfer theory. Ice is very weakly absorptive in the visible (minimum absorption at $\lambda = 0.46$ μm) but has strong absorption bands in the near infrared (near IR). Snow albedo is therefore much lower in the near IR. The near-IR solar irradiance thus plays an important role in snowmelt and in the energy balance at a snow surface. The near-IR albedo is very sensitive to snow grain size and moderately sensitive to solar zenith angle. The visible albedo (for pure snow) is not sensitive to these parameters but is instead affected by snowpack thickness and parts-per-million amounts (or less) of impurities. Grain size normally increases as the snow ages, causing a reduction in albedo. If the grain size increases as a function of depth, the albedo may suffer more reduction in the visible or in the near IR, depending on the rate of grain size increase. The presence of liquid water has little effect per se on snow optical properties in the solar spectrum, in contrast to its enormous effect on microwave emissivity. Snow albedo is increased at all wavelengths as the solar zenith angle increases but is most sensitive around $\lambda = 1$ μm. Many apparently conflicting measurements of the zenith angle dependence of albedo are difficult to interpret because of modeling error, instrument error, and inadequate documentation of grain size, surface roughness, and incident radiation spectrum. Cloud cover affects snow albedo both by converting direct radiation into diffuse radiation and also by altering the spectral distribution of the radiation. Cloud cover normally causes an increase in spectrally integrated snow albedo. Some measurements of spectral flux extinction in snow are difficult to reconcile with the spectral albedo measurements. The bidirectional reflectance distribution function which apportions the reflected solar radiation among the various reflection angles must be known in order to interpret individual satellite measurements. It has been measured at the snow surface and at the top of the atmosphere, but its dependence on wavelength, snow grain size, and surface roughness is still unknown. Thermal infrared emissivity of snow is close to 100% but is a few percent lower at large viewing angles than for overhead viewing. It is very insensitive to grain size, impurities, snow depth, liquid water content, or density. Solar reflectance and microwave emissivity are both sensitive to various of these snowpack parameters. However, none of these parameters can be uniquely determined by satellite measurements at a single wavelength; a multichannel method is thus necessary if they are to be determined by remote sensing.

CONTENTS

A. INTRODUCTION

An understanding of the reflection, absorption, and transmission of light by snow is important for two general applications. The first is the calculation of the radiation budget of snowpacks and the planetary radiation budget over snow-covered surfaces. This is important both for hydrology, because radiation is usually the dominant component in the surface energy budget of snow, and for global climate modeling. The second application is for planning the remote sensing of snowpack properties. This requires modeling of the optical properties at high spectral detail.

Considerable progress has recently been made in under-

[1] Now at Department of Atmospheric Sciences, University of Washington, Seattle, Washington 98195.

Paper number 1R1505.
0034-6853/82/001R-1505$06.00

standing the optical properties of snow in the solar and infrared regions of the spectrum. The most recent review article was that of *Mellor* [1977]. However, the modeling papers of *Wiscombe and Warren* [1980*a*] (hereafter WWI) and *Warren and Wiscombe* [1980] (hereafter WWII) included considerable review material. They reviewed earlier theoretical models, snow albedo observations, and the complex index of refraction of ice and reviewed (where necessary to compare with model results) observations of the dependence of snow albedo on wavelength, grain size or age, liquid water content, solar zenith angle, cloud cover, snowpack thickness, and snow density.

This article gives a more thorough review of observations and modeling than did WWI, treats flux extinction and bidirectional reflectance as well as albedo, but especially reviews the considerable work done since WWI and WWII were written, pointing out topics for further research where theories and observations are lacking or in conflict.

This review of optical properties is limited to the parts of the electromagnetic spectrum which are important for determining the climatic role of snow and for affecting snowmelt. These are the solar ($0.3 \leq \lambda \leq 5$ μm) and thermal infrared ($5 \leq \lambda \leq 40$ μm) wavelengths. (Radiation of wavelength shorter than 0.3 μm is absorbed in the upper atmosphere and does not reach the surface.) Other parts of the spectrum (microwaves) will be mentioned only for the purpose of contrastive analysis in the discussion of the far-field assumption in scattering theory and in the discussion of remote sensing.

B. Definitions

Definitions for reflectance are given by *Siegel and Howell* [1972, pp. 47–88] and by *Nicodemus et al.* [1977].

The reflected radiation is not perfectly diffuse but is unevenly distributed among the reflection angles according to the bidirectional reflectance distribution function (BRDF). This function R has units sr^{-1}:

$$R(\theta_0, \theta', \phi_0, \phi', \lambda) = \frac{dI(\theta', \phi', \lambda)}{\mu_0 dF(\theta_0, \phi_0, \lambda)}$$

where (θ_0, ϕ_0) is the incident (zenith, azimuth) angle, $\mu_0 = \cos \theta_0$, (θ', ϕ') the reflection angle, λ the wavelength, F the incident flux (on a surface normal to the beam), and I the reflected intensity. Unless the surface has azimuthally dependent surface features, such as the sastrugi oriented with their long axes parallel to the prevailing wind at the south pole [*Carroll and Fitch*, 1981], the dependence of R on both ϕ_0 and ϕ' reduces to a dependence only on the relative azimuth $\phi_0 - \phi'$.

The albedo a_s is the 'spectral directional-hemispherical reflectance'; it is the integral of R over all reflection angles:

$$a_s(\theta_0, \lambda) = \int_0^1 \mu' \, d\mu' \int_0^{2\pi} R(\theta_0, \theta', \phi', \lambda) \, d\phi'$$

More simply stated, the albedo is just the upflux divided by the downflux at a particular wavelength, usually measured just above the snow surface.

The albedo for hemispherically isotropic incident radiation is the diffuse albedo a_d:

$$a_d(\lambda) = 2 \int_0^1 \mu_0 a_s(\mu_0, \lambda) \, d\mu_0$$

In general, the albedo depends on the distribution of incident radiation with angle.

The spectrally integrated albedo is what is measured by unfiltered radiometers:

$$\bar{a}_s(\theta_0) = \frac{\int a_s(\theta_0, \lambda) F\downarrow(0, \lambda) \, d\lambda}{\int F\downarrow(0, \lambda) \, d\lambda}$$

where $F\downarrow(0, \lambda)$ is the spectral downflux of solar radiation at the surface. The value of $\bar{a}$ thus depends not only on the snow properties and on the sun angle but also on the atmospheric composition (water vapor content, cloud thickness, etc.), which affects the spectral distribution of the sunlight.

It is often convenient to normalize the bidirectional reflectance relative to the albedo. Thus in Figure 14 below is plotted not R but rather the anisotropic reflectance function f:

$$f(\theta_0, \theta', \phi' - \phi_0) = \pi R(\theta_0, \theta', \phi' - \phi_0)/a_s(\theta_0) \qquad (1)$$

The spectral emissivity $\varepsilon(\theta, \lambda)$ depends on emission angle θ and is equal to the absorptivity or the coalbedo $[1 - a_s(\theta_0, \lambda)]$ by Kirchhoff's law [*Siegel and Howell*, 1972].

Deep in a homogeneous snowpack (uniform density and grain size distribution and far from any boundaries) the spectral flux $F\downarrow(\lambda)$ is attenuated approximately exponentially:

$$F\downarrow(\lambda, z + \Delta z) \approx F\downarrow(\lambda, z) e^{-\kappa_s(\lambda)\Delta z}$$

where $\kappa_s(\lambda)$ is the flux extinction coefficient:

$$\kappa_s(\lambda) = -\frac{d \ln F\downarrow(\lambda)}{dz} = \frac{-1}{F\downarrow(\lambda)} \frac{dF\downarrow(\lambda)}{dz}$$

κ_S^{-1} is often reported in units of geometric depth, but it is better expressed in units of liquid equivalent depth in order to avoid effects of snow density variation.

The important quantities for calculating snowmelt are the surface albedo and emissivity. The important quantities for the earth radiation budget are the planetary albedo and the 8- to 12-μm window emissivity. None of these are measured by narrow field of view satellites, which instead measure the planetary bidirectional reflectance R over a particular wavelength band. This can be converted to planetary albedo for the same wavelength band if the anisotropic reflectance function f is known. Further conversion to a surface albedo requires knowledge of the atmospheric vertical structure.

Other symbols used in the paper are as follows:

$g(x, m)$	single-scattering asymmetry parameter;
$\kappa_i(\lambda)$	absorption coefficient of pure, bubble-free, polycrystalline ice;
$\kappa_s(\lambda)$	flux extinction coefficient for snow;
$m(\lambda) = m_{re}(\lambda) - im_{im}(\lambda)$	complex refractive index of ice;
$Q_{ext}(x, m)$	single-scattering extinction efficiency;
r	snow grain radius;
x	size parameter, equal to $2\pi r/\lambda$;
ρ_s	snow density;
$\tilde{\omega}$	single-scattering albedo.

C. Optical Constants of Ice

Theoretical models of the optical properties of snow require as input the laboratory measurements of the refrac-

tive index m_{re} and absorption coefficient κ_i of pure ice as functions of wavelength. They are combined as the complex index of refraction $m = m_{re} - im_{im}$, where $\kappa_i = 4\pi m_{im}/\lambda$.

Of particular importance for solar albedo calculations are the recent measurements of $\kappa_i(\lambda)$, $0.4\ \mu m \le \lambda \le 1.4\ \mu m$, by *Grenfell and Perovich* [1981]. The absorption coefficient is so small in the visible wavelengths that, to measure it accurately, blocks of bubble-free ice as long as 2.8 m had to be grown in order to obtain sufficient light attenuation.

For $1.4 \le \lambda \le 2.8\ \mu m$ we recommend the values of $m(\lambda)$ compiled by WWI, and for $2.8 \le \lambda \le 33\ \mu m$ we recommend the measurements by *Schaaf and Williams* [1973]. The optical constants of ice from 45-nm to 8.6-m wavelength are reviewed by S. G. Warren (unpublished manuscript, 1981).

D. Measurements of Reflection and Transmission of Light by Snow

1. *Albedo*

All-wave albedo has been routinely measured on polar expeditions for many years. Time series of albedo show high all-wave albedos (75–90%) in late winter and early spring, dropping as snowmelt begins to about 60%. Such time series have been reported for Greenland by *Ambach* [1963] and *Diamond and Gordel* [1956]; for Barrow (Alaska) by *Maykut and Church* [1973]; for McCall Glacier (Brooks Range, Alaska) by *Wendler and Weller* [1974]; for McGill Ice Cap (Canada) by *Havens* [1964]; and for snow-covered sea ice in the Antarctic by *Weller* [1968] and in the Arctic by *Langleben* [1971]. Summaries of monthly average or seasonal average all-wave albedos have been reported for Antarctic stations by *W. Schwerdtfeger* [1970, p. 258] and for drifting ice islands in the Arctic by *Chernigovskii* [1963, p. 269]. For the Antarctic Plateau, where snow never melts, Schwerdtfeger found that 'a useful value of 0.8 as the lower limit of surface albedo appears to be certain.'

Apart from these routine measurements, problem-directed research has sought to identify the factors influencing snow albedo. The albedo of both dry snow and melting snow is normally found to increase as solar zenith angle increases, as measured by *Hubley* [1955], *Liljequist* [1956], *Rusin* [1961], *Bryazgin and Koptev* [1969], *Korff et al.* [1974], and *Carroll and Fitch* [1981]. These measurements are examined in section J2 below. Some workers, however, found the opposite trend. *Havens* [1964] reported highest albedos at midday, as did *Kondratiev et al.* [1964].

Cloud cover affects both the spectral distribution of irradiance and the effective incident zenith angle. It normally causes an increase in all-wave snow albedo. An increase of 5–10% relative to clear-sky albedo was found by *Liljequist* [1956] and 11% by *Weller* [1968], both on the Antarctic coast, and 5–7% by *Hanson* [1960] at the south pole. However, *Carroll and Fitch* [1981] have now found cloud cover to reduce albedo at the south pole; this can be attributed to the unusually steep dependence of albedo on zenith angle which they find, described in section J2 below. *Grenfell et al.* [1981] found snow albedo to increase with cloud optical thickness at a mid-latitude site.

The effect of snow thickness on the albedo of a thin snowpack over a black surface was investigated by *Giddings and LaChapelle* [1961] for monochromatic light at $\lambda = 0.59\ \mu m$. They found the snow albedo to reach within 3% of its asymptotic value at a depth of 8 cm (liquid equivalent), as did *O'Neill and Gray* [1973] for broadband-filtered sunlight, 0.3–1.1 μm. However, *Warren and Wiscombe* [1980, p. 2742] think that these snow samples were probably somewhat contaminated and that pure snow would require 4 times this thickness to reach within 3% of the semi-infinite albedo.

The reduction of albedo due to snow aging has been documented for visible wavelengths by *Holmgren* [1971] and *Grenfell and Maykut* [1977] and for the near IR by *O'Brien and Munis* [1975]. *Grenfell et al.* [1981] studied the progress of spectral albedo changes ($0.4 \le \lambda \le 2.5\ \mu m$) due to snow aging.

Spectrally detailed measurements are necessary for an understanding of the physical processes affecting snow albedo. Many of these measurements were reviewed by WWI and WWII. The most accurate measurements are probably the following. Albedo measurements in four spectral bands for clean Antarctic snow were made by *Liljequist* [1956]. High spectral resolution albedo measurements were reported for $0.4 \le \lambda \le 1.0\ \mu m$ on the Arctic Ocean by *Grenfell and Maykut* [1977], for $0.4 \le \lambda \le 1.5\ \mu m$ at South Pole Station by *Kuhn and Siogas* [1978], for $0.4 \le \lambda \le 2.5\ \mu m$ in the Cascade Mountains by *Grenfell et al.* [1981], and for $0.34 \le \lambda \le 1.1\ \mu m$ on the Great Lakes by *Bolsenga* [1981].

Grenfell and his colleagues have developed a portable (16 kg) scanning spectrophotometer for field measurements. The instrument described by *Roulet et al.* [1974] was useful for $0.4 \le \lambda \le 1.0\ \mu m$; it has been improved by *Grenfell* [1981] with the use of a circular variable interference filter for $\lambda < 1.375\ \mu m$ (resolution $\Delta\lambda \le 0.03\ \mu m$) and fixed wavelength filters to extend the wavelength range out to 2.45 μm ($\Delta\lambda \approx 0.1\ \mu m$).

2. *Bidirectional Reflectance*

The bidirectional reflectance measurements of *O'Brien and Munis* [1975] were designed principally to investigate the spectral dependence of reflectance for $0.6 \le \lambda \le 2.5\ \mu m$; only a narrow range of incidence and detector angles was employed. Although they are not albedo measurements, they were used as proxy evidence for near-IR spectral albedo and its dependence on snow age by the albedo-modeling efforts of *Choudhury and Chang* [1979*a*, *b*] and *Wiscombe and Warren* [1980*a*].

Measurements of spectrally integrated bidirectional reflectance over a large range of angles were made by *Dirmhirn and Eaton* [1975]. Measurements over a restricted range of angles but for a variety of snow types were reported by *Middleton and Mungall* [1952]. Section L below reviews these as well as the aircraft measurements of *Griggs and Marggraf* [1967] and *Salomonson and Marlatt* [1968*a*, *b*]. The dependence of the BRDF on wavelength, grain size, and surface irregularity has not been adequately studied either experimentally or theoretically.

3. *Flux Extinction*

The monochromatic flux extinction coefficient $\kappa_s(\lambda)$ decreases rapidly with depth near the surface where a significant fraction of the upwelling radiation escapes the snowpack. Below a few centimeters depth the effect of the top boundary is no longer noticeable, and one measures an 'asymptotic' monochromatic flux extinction coefficient which is independent of depth for a homogeneous snowpack. The asymptotic flux extinction coefficient has been mea-

TABLE 1. Models for the Optical Properties of Snow

Reference	Input Parameters	Grain Size Enters	Wavelength Dependence Examined	Anisotropic Scattering Considered	Sun Angle Dependence	Thin Snow Treated	Comments
Dunkle and Bevans [1956]	t, m	as t	yes			yes	for diffuse incidence and high albedo
Giddings and LaChapelle [1961]	l, m_{im}	as l				yes	for diffuse incidence and high albedo
Barkstrom [1972]	$\tilde{\omega}, \theta_0$				yes		must be tuned
Barkstrom and Querfeld [1975]	$\tilde{\omega}$, g, θ_0	yes		yes	yes	yes	unrealistic g
Bohren and Barkstrom [1974]	r, m	yes		yes			for diffuse incidence and high albedo
Berger [1979]	m, ρ_s	yes	yes	yes			for high infrared emissivity
Choudhury and Chang [1979*a*, *b*]	r, m, β	yes	yes	yes		yes	for diffuse incidence and albedo $\gtrsim 0.1$
Wiscombe and Warren [1980*a*]	r, m, θ_0	yes	yes	yes	yes	yes	used in this paper
Choudhury and Chang [1981]	r, m, θ_0, s^2	yes	yes	yes	yes		'surface reflection' included

Symbols used are as follows: g, single-scattering asymmetry parameter; l, photon mean path length through ice; $m = m_{re} - im_{im}$, complex index of refraction of ice; r, snow grain radius; s^2, variance of surface facet slopes; t, ice lamina thickness; β, single-scattering backscattered fraction; θ_0, solar zenith angle; ρ_s, snow density; and $\tilde{\omega}$, single-scattering albedo.

sured as a function of wavelength by *Liljequist* [1956] and with better spectral resolution by *Grenfell and Maykut* [1977] and *Kuhn and Siogas* [1978]. These relatively monochromatic measurements are better suited to testing theoretical models than are all-wave extinction measurements and are discussed below in section I2.

Only a few such monochromatic measurements of flux extinction have been reported. Far more commonly measured is the attenuation of all-wave solar radiation in snow, which has been reported by (among others) *Ambach and Habicht* [1962], *Ambach* [1963], *Weller* [1969], and *Schwerdtfeger and Weller* [1977]. A number of other measurements were reviewed by *Mellor* [1977], who also clearly explained intuitively the fact that κ_s decreases as grain size increases. Unlike the monochromatic $\kappa_s(\lambda)$ the all-wave κ_s does not quickly reach an asymptote. It decreases with depth because of the changing spectral composition of sunlight with depth. At great depth, where all but the blue light is filtered out by the snow, κ_s will reach the asymptotic value corresponding to $\lambda = 0.46$ μm.

4. *Intensity Extinction*

The extinction and scattering of a directed beam of monochromatic radiation as a function of angle and depth in the snowpack has been studied by Ambach and his coworkers [e.g., *Ott*, 1974]. These measurements could be useful for testing future models which may attempt to calculate intensities as well as fluxes within the snowpack.

E. MODELING THE OPTICAL PROPERTIES OF SNOW

Modeling of the reflection and transmission of light by snow has nearly a 30-year history. A rather oversimplified summary is given in Table 1. The early models of *Dunkle and Bevans* [1956] (hereafter DB) and *Giddings and LaChapelle* [1961] did not explicitly compute scattering by individual ice grains but set up a two-stream radiative transfer framework which required two input parameters. These two parameters can be loosely related to an effective grain size and an absorption coefficient, but they are normally found by fitting experimental data. Because these models are computationally simple, they have been used extensively for fitting albedo and flux extinction data [e.g., *Weller*, 1969; *P. Schwerdtfeger*, 1969; *Bergen*, 1970, 1971, 1975; *Schlatter*, 1972; *O'Neill and Gray*, 1973]. However, they are not generally applicable outside the wavelength range where they are tuned.

The application of modern radiative transfer theory to snow was pioneered by Barkstrom and Bohren, who started with the single scattering by individual ice sphere and used a number of approximations to relate these to observable quantities. *Bohren and Barkstrom* [1974] (hereafter BB) obtained very simple equations which (as shown below) are applicable only for the visible wavelengths. *Choudhury and Chang* [1979*a*] also started with single scattering by ice particles and used a two-stream method for radiative transfer. They did not attempt to derive simple parameterizations as had BB. Their model is applicable over a wider wavelength range than is BB's and is more accurate than the model of DB.

The most accurate model now available for computing radiant fluxes in snow (short of a much more costly doubling or discrete ordinates method) is the delta-Eddington/Mie theory model used by WWI. Although we sometimes use it in this section as a benchmark to criticize other models, one should keep in mind that the WWI model still has shortcomings, which are discussed in later sections of this paper: it neglects effects due to close packing (which restricts its validity to $\lambda \lesssim 20$ μm) and nonsphericity of snow grains (which may cause errors at very large solar zenith angles $\theta_0 \rightarrow 90°$), and it calculates only fluxes, not intensities, so it says nothing about the BRDF. However, it has proven very useful in explaining quantitatively the influence of snow parameters and environmental parameters on spectral albedo.

1. *Early Two-Stream Models*

Dunkle and Bevans modeled the snowpack as a stack of horizontal ice layers. They calculated the Fresnel reflection

at normal incidence on each layer, as well as the absorption of light passing vertically through the layer according to *Sauberer*'s [1950] measurements of κ_i. Given these reflection and absorption coefficients, as a function of wavelength, they used the Schuster two-stream method to examine the dependence of albedo on the thickness of the ice layers. In Figure 1 we reproduce Figure 3 of DB together with the more accurate calculations of the Wiscombe-Warren model, assuming that DB's layer thickness represents the snow grain diameter. The DB model gives the correct qualitative behavior of $a_d(r, \lambda)$, showing the decrease of albedo due to increased grain size as the snow ages, as well as the fact that albedo is lower in the near IR than in the visible. However, there are substantial errors. These errors are due to treating the ice as sheets rather than as particles, the assumption of normal incidence Fresnel reflectivity, and the use of two-stream theory (An additional small part of the discrepancy is due to the WWI model's use in Figure 1 of the new measurements of m_{im} by *Grenfell and Perovich* [1981].)

DB gave formulas for both albedo and transmittance for both thin snow and semi-infinite snow. Although they obtained their absorption and reflection coefficients from laboratory mesurements on pure ice, later users of their model have treated these coefficients as two adjustable parameters to be fit to field observations of snow.

Giddings and LaChapelle [1961] (hereafter GL) used a diffusion model which, like DB's, also employs two adjustable parameters, a diffusion coefficient and an absorption coefficient. The GL model is actually equivalent to the DB model, because the diffusion approximation is a form of two-stream approximation. (Recently, both *Meador and Weaver* [1980] and *Zdunkowski et al.* [1980] have shown that all two-stream approximations are equivalent and can be put into a common framework.) The diffusion coefficient was related to a length l which is the average distance a photon travels through ice between air-ice interfaces, so it is interpreted as the effective grain diameter. GL estimated that the simple diffusion model was accurate if there were a large number of scatterings before the absorption of a photon, that is, if $a_d \gtrsim 0.8$. Correcting for 'nondiffuseness' (taking into account the nonunit ratio of downflux to upflux, $F\uparrow/F\downarrow < 1$) was thought to extend the validity of the model down to albedo as low as 0.5.

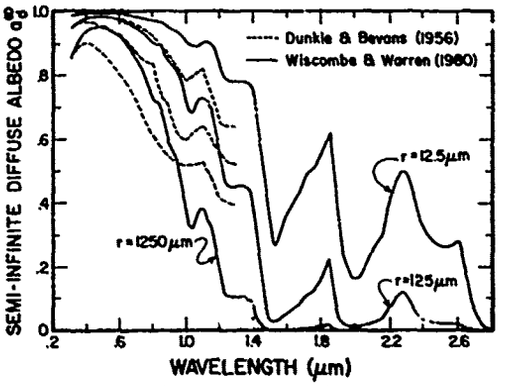

Fig. 1. Model calculations of semi-infinite diffuse albedo as a function of wavelength for various snow grain radii. Dashed lines are calculations by *Dunkle and Bevans* [1956, Figure 3]. Solid lines are calculations using the model of WWI, with the new m_{im} (λ) measured by *Grenfell and Perovich* [1981].

For small absorption (large albedo), equations 13 and 21 of GL imply that $1 - a_d \propto r^{1/2}$, a result also obtained later by *Bohren and Barkstrom* [1974].

GL made measurements of albedo and transmission of thin snow over a black background for monochromatic light ($\lambda = 0.59$ μm) to determine the two free parameters in the diffusion model. They found the same two parameters to fit both the albedo data and the transmission data. However, the value of l obtained was 20 times the grain radius estimated by eye, $l = 20r$, whereas it should be $l = 2r$ according to the interpretation of l as grain diameter.

GL also analyzed the disturbance of the radiation field due to a radiometer inserted into the snow. The instrument measures less downflux than would be present in the undisturbed snow because it is blocking some of the upflux that otherwise could be scattered back down. This is one of the reasons why transmission measurements are more difficult than albedo measurements.

2. *Single-Scattering by Ice Grains Introduced*

The scattering and absorption of radiation by a single ice particle are described by three quantities:

1. Extinction efficiency Q_{ext} is the ratio of the extinction cross section to the geometric cross section. For large particles ($r \gg \lambda$), Q_{ext} is close to its geometric optics limit of 2.

2. Single-scattering albedo $\tilde{\omega}$ is the ratio of scattering efficiency to extinction efficiency. It is the probability that a photon intercepted by a particle will be scattered rather than absorbed.

3. Phase function $P(\Omega_1, \Omega_2)$, when multiplied by $\tilde{\omega}$, gives the probability that a photon incident from angle $\Omega_1 = (\theta_1, \phi_1)$ will be scattered into angle $\Omega_2 = (\theta_2, \phi_2)$. For a spherical particle, P is a function only of the cosine of the scattering angle $\Omega_2 \cdot \Omega_1$. The complete phase function is needed for computing intensity, but for computing fluxes normally only a single measure of the anisotropy of P is needed, commonly the asymmetry parameter g, which is the mean value of $\Omega_2 \cdot \Omega_1$, or the backscattered fraction β [*Wiscombe and Grams*, 1976; *Zdunkowski et al.*, 1980].

Both $\tilde{\omega}$ and g are dimensionless with ranges $0 \le \tilde{\omega} \le 1$ and $-1 \le g \le 1$; $g = 0$ corresponds to isotropic scattering, and $g = 1$ to completely forward directed scattering.

Barkstrom [1972] assumed the snowpack to be semi-infinite, grey, and isotropically scattering. He introduced a zenith angle dependence by solving the radiative transfer equation for intensity. This was then integrated to get flux in terms of the X functions of radiative transfer. He calculated that albedo would increase with zenith angle in approximate agreement with measurements of *Rusin* [1961] and *Liljequist* [1956]. He also showed that the (monochromatic) flux should decrease faster than exponentially at the surface but at great depth should decrease exponentially, $dF\downarrow/dz = -\kappa_s F\downarrow$, with κ_s independent of solar zenith angle.

The first consideration of the anisotropic scattering by ice grains was that of *Barkstrom and Querfeld* [1975], who attempted to explain the bidirectional reflectance measurements of snow by *Middleton and Mungall* [1952]. Barkstrom and Querfeld used the adding-doubling method for radiative transfer. However, in order to match Middleton and Mungall's measurements they required quite unrealistic values of asymmetry parameter ($g = 0.5$, corresponding to $r = 0.1$ μm,

whereas $g \approx 0.9$ for a realistic grain size $r > 50$ μm).

Bohren and Barkstrom [1974] used geometrical optics in the limit of small absorption to calculate the scattering by individual ice spheres. They obtained $g = 0.874$, close to the asymmetry parameter found in exact Mie calculations for a wide range of particle sizes ($g \approx 0.89$ for $\lambda < 1$ μm in Figure 4 of WWI). The geometrical optics calculation also showed that the scattered light was due mostly to refraction rather than reflection.

BB made a number of approximations which used the assumption that $\kappa_i r \ll 1$, which means that their results apply only to the visible wavelengths. They obtained simple formulas for albedo under isotropic illumination,

$$a_d = 1 - 8.43(\kappa_i r)^{1/2} \quad (2)$$

and for asymptotic flux extinction coefficient,

$$\kappa_s = 0.65(\kappa_i / r)^{1/2} \quad (3)$$

where depth is measured as liquid-equivalent depth. Neither (2) nor (3) involves snow density. (BB's formula did show κ_s to be proportional to snow density, but this dependence disappears if we measure depth as liquid-equivalent depth. We do this in order to investigate possible near-field effects which are ignored in all published models and which would introduce a density dependence into (2) and (3), as discussed in section E5 below.)

Figures 2 and 3 compare equations (2) and (3) with the more accurate results of WWI for several wavelengths. Figure 2 shows that the albedo is indeed proportional to $r^{1/2}$ for $\lambda < 0.8$ μm. Accordingly, BB found good agreement of (2) with *Liljequist*'s [1956] observations of high visible albedo ($a_d \approx 0.96$) using Liljequist's measured grain size $r = 15$ μm; this is the wavelength region where (2) is applicable. However, (2) becomes useless as ice becomes more absorptive in the near IR. At $\lambda = 1.3$ μm, for example, (2) predicts negative albedos for $r > 110$ μm. Figure 3 shows that the flux extinction formula (3) is better behaved than the albedo formula. The results of the WWI model show that $\kappa_s \propto r^{-1/2}$, as (3) predicts, but that the WWI model increasingly deviates from (3) as $\kappa_i(\lambda)$ increases ($\kappa_i(1.5) > \kappa_i(1.8) > \kappa_i(1.3$ μm)). It may be that snow albedo and flux extinction can be parameterized by simple formulas like (2) and (3), but more work is needed to develop parameterizations that are applicable over wider wavelength ranges.

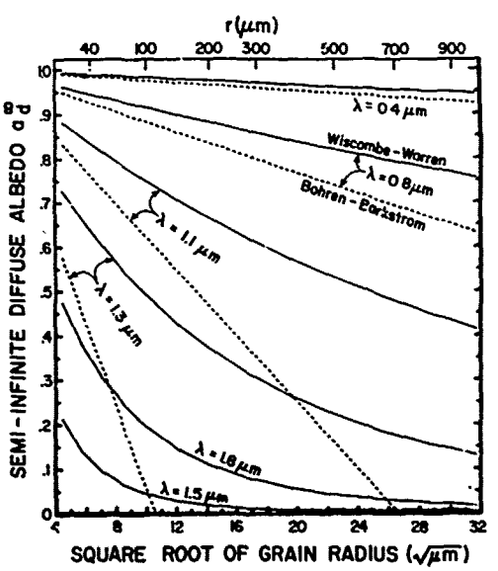

Fig. 2. Diffuse albedo versus square root of grain radius for six discrete wavelengths. Solid lines are calculated using WWI model. Dashed lines are calculated using equation (42) of *Bohren and Barkstrom* [1974].

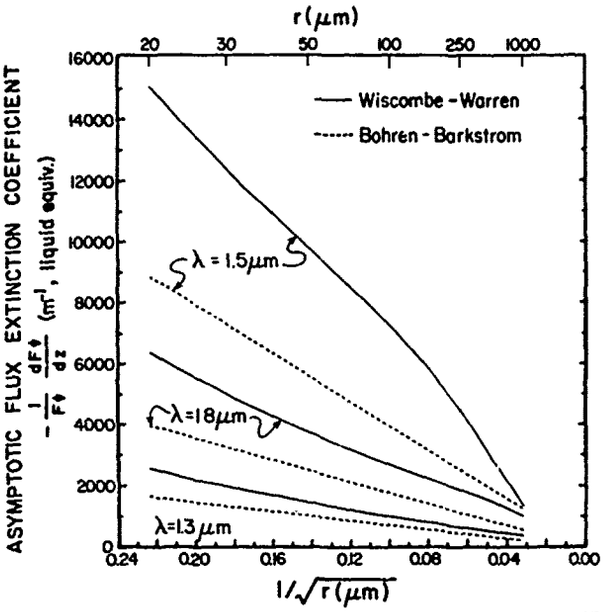

Fig. 3. Asymptotic flux extinction coefficient κ_s versus $(1/r)^{1/2}$ for three discrete wavelengths. Solid lines are calculated using WWI model. Dashed lines are calculated using equation (37) of *Bohren and Barkstrom* [1974].

Berger [1979] adapted the Bohren-Barkstrom theory for the limit of large absorption, assuming that any photon entering an ice sphere is absorbed by it. This assumption makes the optical properties independent of grain size. Berger's interest was to model the infrared emissivity of snow, and his large-absorption approximation is reasonable for $r > 100$ μm in the thermal infrared, as we show below in section M1. Berger found the emissivity ε to depend on snow density ρ_s, with ε increasing as ρ_s decreases, owing to the reduced average angle of incidence on spheres in a regular array. This may be unrealistic, because the derivation depends on the particular spherical shape of ice grains and on the assumption that they are in a regular array. However, Berger found the dependence of ε on ρ_s to be weak (Figure 17 below).

The next experimental advances which stimulated further modeling were the spectral bidirectional reflectance measurements of *O'Brien and Munis* [1975]. *Choudhury and Chang* [1979*a*, *b*] (hereafter CCa and CCb) used the Sagan-Pollack two-stream model, which was rather good at all wavelengths, and they obtained tolerable agreement with O'Brien and Munis' measurements (uncorrected for the reflectance of the $BaSO_4$ standard). In contrast to the models of DB, GL, and BB, none of which were applicable for $a_d < 0.5$, the Choudhury-Chang model became inaccurate only for $a_d \lesssim 0.1$ (compare Figure 4 of CCa with Figure 1 of CCb). In their two-stream model, CC assumed a backscatter fraction (7.5%) independent of wavelength, using single-scatter-

ing albedo calculated from r and m_{im} by means of a parameterization due to *Sagan and Pollack* [1967]: $\tilde{\omega} = \frac{1}{2} + \frac{1}{2}\exp(-b\kappa_i r)$, where b is an adjustable parameter taken as $b = 1.67$ by CCa and as $b = 2.0$ by CCb. These approximations make the CC two-stream model more accurate than the DB two-stream model. In CCb a 'surface reflection' term was introduced which calculated the Fresnel reflection from a flat sheet of ice at the snow surface. However, the performances of the two CC models were not compared with each other in either of these papers, so the effect of the hypothetical surface layer is not clear.

3. *Wiscombe-Warren Model*

The advances in modeling made by WWI were to use Mie scattering theory, which made the single-scattering calculations accurate at all wavelengths and for all grain sizes, and to use the delta-Eddington approximation [*Joseph et al.*, 1976] to handle the anisotropic phase function, which allowed the model to calculate albedo for any solar zenith angle and for an arbitrary mix of diffuse and direct radiation. The detailed measurements of visible spectral albedo by *Grenfell and Maykut* [1977] further inspired WWII to adapt their model to calculate the effect of absorptive impurities on snow albedo.

The snowpack was modeled as ice spheres, and it is argued by WWI why the effects of nonsphericity should be small in relation to the effects of grain size variation. The scattering and absorption of light by single ice spheres is described by Mie theory. Mie calculations, even using the fast algorithms of *Wiscombe* [1980], are extremely time consuming for the larger snow grain sizes. However, for these large grains (actually for any grains whose size parameter is $x \geq 100$, where x is the ratio of the circumference of the sphere to the wavelength of light), asymptotic formulae have been developed [*Nussenzveig and Wiscombe*, 1980] which are sufficiently accurate and much faster than the Mie calculations.

Mie theory assumes that the particles behave as isolated scatterers. If they are not sufficiently separated, then near-field effects will be observed that are not predicted by Mie theory. WWI examined this question in their section 7 and concluded that the near-field effects are probably negligible for snow in the solar spectrum. They become important at longer wavelengths, and a criterion for estimating them is described below in section E5.

The single-scattering quantities Q_{ext}, $\tilde{\omega}$, and g at a particular wavelength are functions of the complex refractive index m and the effective snow grain radius r. (This is the area-weighted mean radius, which is always larger than the number-weighted mean radius.) These single-scattering quantities become the input to a multiple-scattering model. A logical model for snow albedo is the delta-Eddington method, because it can adequately handle the extreme asymmetry of scattering by ice particles in snow, in which a large fraction of the scattered light is only slightly deflected. The delta-Eddington method is designed to be efficient and accurate for calculating radiant fluxes.

The model can also be used to calculate snow infrared emissivity as described below in section M.

The wavelength dependence of snow albedo is controlled by the variation with wavelength of the absorption coefficient of ice $\kappa_i(\lambda)$. Within that constraint the model shows that snow spectral albedo is highly sensitive to grain size and moderately sensitive to solar zenith angle and, in the visible wavelengths only, to trace amounts of absorptive impurities. The principal results of the model are summarized in the appropriate sections below.

4. *Choudhury-Chang Model*

Choudhury and Chang [1981] (hereafter CC81) and *Choudhury* [1981] have now abandoned the two-stream approach in favor of the delta-Eddington method. (*Dozier et al.* [1981] have shown that although not obvious, equation (28) of CC81 is indeed equivalent to equation (4) of WWI. This is the special case of direct incidence on a semi-infinite snowpack, where a_r^∞ is a function of only the three parameters $\tilde{\omega}$, g, and μ_0.)

Instead of doing Mie calculations, CC81 used the Sagan-Pollack approximation for $\tilde{\omega}$ mentioned above and a parameterization for g which they devised to mimic some published results from Mie theory. However, these approximations are quite good at mimicking the Mie results, at least for the larger grain sizes. Thus the spectral albedo calculations of CC81 would be nearly identical to those of WWI, except for the use by CC81 of a special 'surface reflection' term. This feature of the CC81 model has been criticized by *Warren and Wiscombe* [1981], who think that CC81's special accounting of surface reflection is unnecessary for ordinary snow in the solar spectrum. Warren and Wiscombe's main points are as follows: (1) The nature of the interaction of electromagnetic radiation with a snowpack depends on the ratio d/λ, where d is the interparticle (center to center) separation; snow does exhibit a 'surface' to radio waves but not to sunlight. (2) Even if one does want to include a surface reflection treatment for special situations that would require it, it is formulated incorrectly by CC81. (3) The reason for introducing surface reflection, namely, to match wavelength-integrated albedo observations, is insufficient, because the model-measurement discrepancy could in this case be due to errors in the atmospheric radiation model instead of the snow albedo model.

There is also no need to invoke a special surface reflection to explain the enhanced specular reflection peak at low sun angle. The explanation for specular reflection in terms of standard single-scattering and multiple-scattering theory is included below in the section on zenith angle dependence (section J).

Although CC81's use of a surface reflection term for a homogeneous snowpack of small, randomly oriented grains seems inappropriate, such a separate modeling of surface reflection could indeed be required for a highly nonrandom surface, in particular for the case of glazed crust, or 'firnspiegel' [*LaChapelle*, 1969, Figures 59 and 60].

5. *Neglected Effects*

a. Near-field effects. Because snow particles are closely packed, they may be in each other's 'near field,' meaning that Mie scattering theory is inapplicable. The problem of near-field interference was mentioned by BB, who cited experiments by *Blevin and Brown* [1961] on the density dependence of the albedo of pigments as evidence that near-field effects would be unimportant for densities of $\rho_s < 0.45$ g cm^{-3}. But in these experiments, $r \approx \lambda$; it is likely that near-field effects can be ignored in snow up to considerably higher

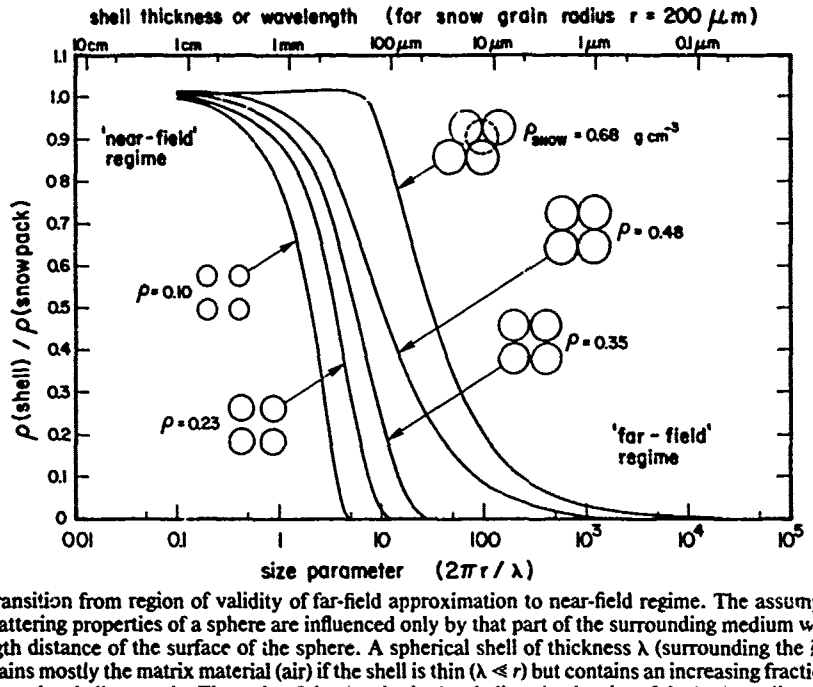

Fig. 4. Transition from region of validity of far-field approximation to near-field regime. The assumption is made that single-scattering properties of a sphere are influenced only by that part of the surrounding medium which is within one wavelength distance of the surface of the sphere. A spherical shell of thickness λ (surrounding the ice particle of radius r) contains mostly the matrix material (air) if the shell is thin ($\lambda \ll r$) but contains an increasing fraction of ice from other spheres as the shell expands. The ratio of the density in the shell to the density of the bulk medium (spheres plus air) is plotted as a function of size parameter or shell thickness for five different regular arrangements of spheres: (1) hexagonal close packing (ρ_{snow} = 0.68 g/cm^3), (2) simple cubic packing, spheres in contact (ρ_{snow} = 0.48), (3) simple cubic packing, spheres not quite in contact, interparticle gap of 0.22r (ρ_{snow} = 0.35) (4) interparticle gap of 0.56r (ρ_{snow} = 0.23), (5) interparticle gap of 1.33r (ρ_{snow} = 0.10).

density. WWI reviewed the possible near-field effects and pointed out that interparticle interference should be neglected for particles whose center-to-center separation d is large in comparison to the wavelength λ. Since $d \gg \lambda$ in the solar spectrum, no interference should be observed, and this is confirmed by *Bohren and Beschta*'s [1979] observation that the albedo of a thick snowpack is independent of density. For microwaves, where $d \leq \lambda$, interference effects will arise, making snow microwave emissivity a function of snow density. Both $\tilde{\omega}$ and g are altered. It is possible to make a rough estimate of the effect using *Gate*'s [1973] adjustment to Mie theory to investigate this dependence on density. Gate simply altered m_{re} of the medium to be not that of air but rather a volume-weighted mean of m_{re} (air) and m_{re} (ice). The 'medium' should probably be taken to be a shell, one or a few wavelengths thick, surrounding the particle. The transition from the far-field regime to the near-field regime should then be described qualitatively by Figure 4. Roughly stated, snow is safely in the far-field regime for $\lambda < 1$ μm and in the near-field regime for $\lambda > 1$ cm, with a transition region whose location depends on snow density.

It is possible that near-field effects could become important for flux extinction (and for the albedo of thin snow) even when they do not affect the albedo of deep snow. This is because the albedo of deep snow depends on g and $\tilde{\omega}$ but not on Q_{ext}, whereas the asymptotic flux extinction coefficient depends on Q_{ext} as well. Whether the near-field approach of snow grains could in some wavelength region significantly affect Q_{ext} but not g or $\tilde{\omega}$ is an open question.

b. Surface irregularity. The model calculations of albedo all assume that the snow surface is flat. Surface irregularities can reduce the albedo relative to that of a flat surface if the height scale of the irregularities is comparable to or larger than the length scale and if both scales are comparable to or larger than the penetration depth of light (which depends on μ_0). This means that surface roughness of ≳10-cm amplitude (such as suncups) is required to reduce visible albedo but that much smaller irregularities can affect near-IR albedo. The albedo is reduced relative to that of a flat surface because some of the light reflected from a slope does not escape to space but instead is intercepted by the slope facing it. There is, of course, no enhancement of absorption if the albedo of the flat surface is 0.0 or 1.0; the enhancement must reach a maximum at some intermediate value of albedo. *Pfeffer* [1982] has developed a model for use in calculating the enhanced absorption due to glacier crevassing, and his model might be adapted to the study of smaller irregularities.

F. Effect of Snow Grain Size on Albedo

Figure 1 shows the calculated spectral albedo of snow for diffuse incident radiation for three different grain sizes expressed as spherical radii r. These radii were chosen for comparison with Figure 3 of DB, but the smallest size is probably unrealistic. To match reflectance measurements of *O'Brien and Munis* [1975] for new snow, WWI never needed grain sizes smaller than r = 50 μm. What the optically equivalent sphere would be for a nonspherical snow particle is discussed below.

The albedo is very high in the visible wavelengths, corresponding to the minimum in m_{im}, and lower in the near infrared. The albedo drops at all wavelengths as the grain size increases. It is easy to understand why albedo should decrease with increasing grain size. Roughly stated, a photon has a chance to be scattered (or a ray to be bent) when it

crosses an air-ice interface. It has a chance of being absorbed only while it is passing through the ice. An increase in grain size causes an increase in the path length that must be traveled through the ice between scattering opportunities. (A similar dependence of reflectance on sand grain size was found by *Leu* [1977] for beach sand, which is in some ways analogous to snow.)

On the basis of matching the model results to observations of *O'Brien and Munis* [1975] (see Figures 10 and 15 of WWI) the optical grain size of the snow surface generally varies in the range from 50 μm for new snow to 1 mm for old melting snow. This increase of grain size with increasing age is the normal situation, but there can be curious exceptions. *Liljequist* [1956] routinely observed the albedo at Maudheim (on a small ice shelf at the coast of Antarctica) to be low after a new snowfall and to rise after a windstorm. At the very cold temperatures of Maudheim, snow metamorphism apparently proceeds so slowly that grain size changes may be due to other effects. Wind probably caused a reduction in grain size by breaking the crystals and possibly also by gravitational sorting. The latter sould cause the smallest particles to settle out last, so they would end up at the surface, where they would dominate the albedo.

1. *The Optically Equivalent Sphere*

How a field measurement of snow grain size translates into the radius of the optically equivalent sphere is a subject of current research. *O'Brien and Koh* [1981] found that the 'equal projected area' assumption gave an overestimate of the radius of the equivalent sphere. Comparison of *Grenfell et al.*'s [1981] albedo measurements with Figure 1 shows that their report of grain radius as half the minimum dimension of the snow grain is a factor of 2–5 smaller than the optical grain size. The best conversion procedure must lie between these two extremes and is probably that suggested by *Dobbins and Jizmagian* [1966] (and by WWI). Namely, the optically equivalent sphere is that which has the same volume-to-surface ratio V/S as the nonspherical snow particle. The results of *Pollack and Cuzzi* [1980] also suggest this. (In the case of a sphere, of course, all three definitions of grain size converge.)

However, any attempt to treat a nonspherical particle as an equivalent sphere involves a compromise, because the sphere with the correct $\tilde{\omega}$ may not have the correct g. Furthermore, the sphere which gives the correct $\tilde{\omega}$ at one wavelength may not do so at another wavelength. The sphere with the same V/S is likely to be most appropriate at wavelengths where absorption is small, $\kappa_i r \ll 1$.

2. *Grain Size Increasing with Depth*

The albedos in Figure 1 are for a homogeneous snowpack, that is, one whose average grain size does not vary with depth. Grain size is observed to increase with depth in a predictable manner in the Antarctic but can, of course, both increase and decrease with depth at mid-altitudes. In order to affect the shape of the spectral albedo curve the grain size must change rapidly with depth; the most likely situation where this effect would be noticed is for a very thin layer of new snow on a thick layer of old snow. This effect has been calculated by S. G. Warren and W. J. Wiscombe (unpublished data, 1981). An increase of r with depth corresponding to about one-third the rate of increase found in the top centimeter at the south pole [*Stephenson*, 1967, Figure 8], causes a greater decrease in visible albedo than in near-IR albedo. This is due to the greater penetration depth of the visible light, which thus 'sees' a larger average grain size. For faster rates of radius increase with depth, however, another effect takes over. The albedo drops more in the 1-μm region than in the 0.4-μm region. Reference to Figure 1 explains this: the albedo is insensitive to grain size where albedo is very high (0.4 μm) or very low (2.8 μm) but highly sensitive in the region of intermediate albedo (1 μm).

3. *Snow Density*

There have been many reports of snow albedo decreasing as density increases. Neither BB nor WWI nor CC obtained a density dependence in their models. The observed dependence of albedo on density might actually be a dependence on grain size, since density normally increases as grain size increases. *Bohren and Beschta* [1979] isolated the two parameters, finding albedo unchanged when density was artificially increased at presumably constant grain size.

Density enters *Bergen*'s [1975] model as a parameter used in computing the air permeability, which is used to compute V/S, which in turn is used to compute the reflection coefficient in the DB model. We interpreted grain size above as proportional to V/S, so it appears that Bergen's dependence of albedo on density could actually be translated into a grain size dependence, when grain size is defined as above.

G. Effect of Liquid Water Content

WWI cited both experimental and theoretical evidence that the effect of liquid water on snow albedo is simply to increase the effective grain size, because the refractive index contrast between water and ice is very small. We wish only to add a footnote to that statement here. *O'Brien and Koh* [1981] have pointed out that the slight differences (a few percent at some near-infrared wavelengths) in reflectance noted between wet melting snow and the subsequently refrozen snow (Figure 5) are in the right direction and of the right magnitude to be attributed to the difference in spectral m_{im} of water and ice. This is most obvious between 1.2- and 1.4-μm wavelength.

H. Effect of Impurities on Snow Albedo

WWII modeled an impure snowpack as a mixture of ice particles and dust or soot particles. They showed that small amounts of impurities affect snow albedo only in the spectral region where absorption of light by ice is weakest, mainly in the visible ($\lambda < 1$ μm). Reductions of visible albedo by a few percent can be caused by ~10 parts per million by weight (ppmw) of desert dust or ~0.1 ppmw of carbon soot. A given amount of an absorptive impurity causes a greater reduction in albedo for coarse-grained snow than for fine-grained snow, as will be illustrated in Figure 7.

1. *Soot*

WWI and WWII showed that some published low values of visible spectral albedo for apparently clean snow could be explained by the model only if the measured snow sample had contained a grey absorber such as soot. Discrepancies between model and observation were obvious for the recent careful spectral albedo measurements of *Grenfell and May-*

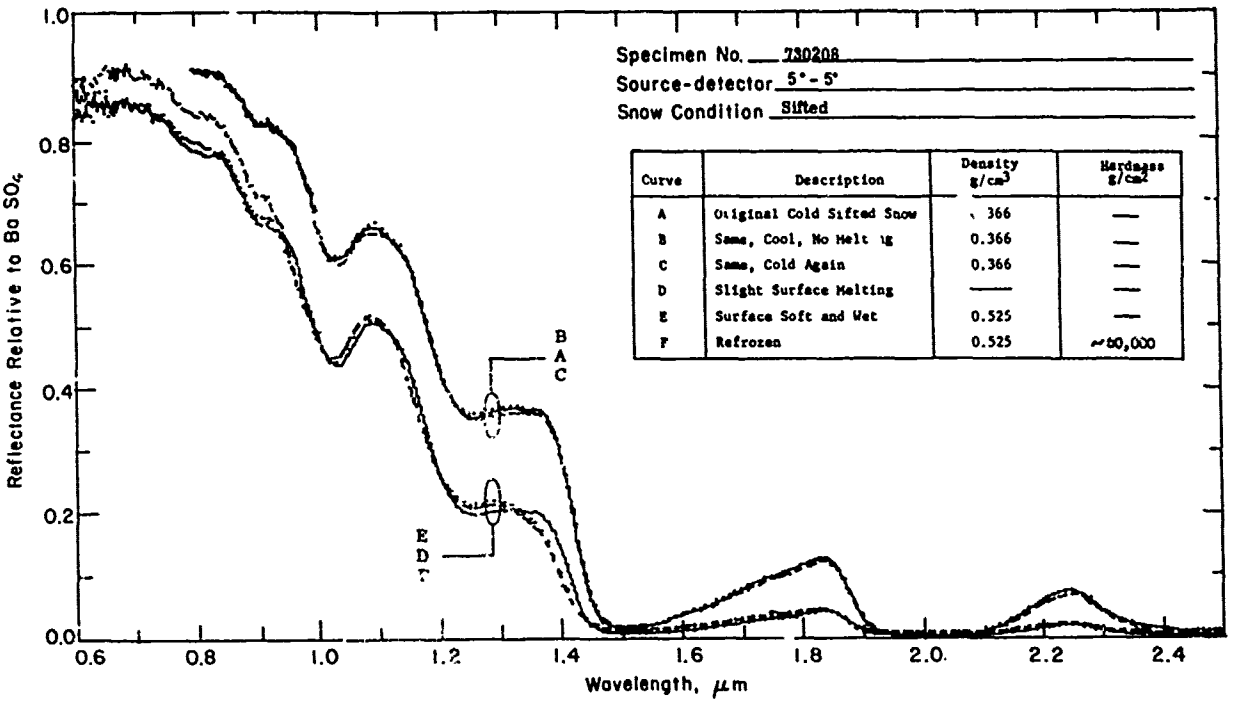

Fig. 5. Effect of liquid water on snow spectral reflectance. (Figure 6 of *O'Brien and Munis* [1975].)

kut [1977] at Arctic ice island T-3 and *Kuhn and Siogas* [1978] at the south pole.

Figure 6 shows that the model for pure snow may predict albedos up to 15% higher than those which are actually observed. Unrealistically large grain sizes could reduce the calculated visible albedo but would destroy the agreement with observation in the near IR. The two major effects which are neglected in the model, namely, nonsphericity of snow grains and near-field scattering, were judged (section 7 of WWI) to be orders of magnitude too small to be responsible for the discrepancy. Insufficient snow depth and error in laboratory-measured ice absorption coefficient were also ruled out as the explanation, leaving impurities as the remaining hypothesis. In order to match the spectral shape of albedo at T-3 (Figure 6) a grey absorber such as soot was implicated, and desert dust was ruled out.

The soot in snow at T-3 may result from pollution, either local or distant. There is soot in the Arctic air [*Rosen et al.*, 1981] which may come from industrial sources in Europe [*Rahn*, 1981], but it is questionable whether the high soot concentrations found necessary to explain snow albedo at T-3 (~0.2 ppmw soot) are representative of the entire Arctic. H. Rosen (personal communication, 1981) found soot amounts in the range 0.01–0.06 ppmw in a preliminary experiment on snow samples from Barrow, Alaska.

We can be fairly certain that any soot at the south pole would be the result of local contamination from the permanent camp. For representative visible spectral albedos for the Antarctic, one should therefore use *Liljequist*'s [1956, Figure 45] high values, which agree with the pure-snow model, rather than Kuhn and Siogas' low values. For $\lambda > 1$ μm, soot has no effect (Figure 1 of WWII), and Kuhn and Siogas' measurements for these wavelengths should be representative of Antarctic snow. They correspond to an average grain radius of 100 μm, which agrees fairly well with *Stephenson*'s [1967, Figure 8] grain size measurements at Southice.

Grenfell et al. [1981] have recently made simultaneous measurements of spectral albedo, grain size, and soot for a snowpack in the Cascade Mountains. We can compare these results with the model of WWII. The measured grain size in this case is much smaller than the effective optical grain size, as mentioned above, so we ignore the grain size data and instead determine the optical grain size from the albedo measurements at $\lambda > 1$ μm, where soot has no effect on albedo. It then appears that in order to explain the visible albedos the WWII model would need 2–5 times as much soot as was actually found in the snow. A factor of 2 difference can be explained by reconciling the definitions of soot amount. (The effect of a given weight fraction of soot on snow albedo depends on the assumed values of absorption coefficient and density for soot. Grenfell et al. used an operational definition of soot concentration which assumes a mass absorption coefficient of 8 $m^2 g^{-1}$ at $\lambda = 0.55$ μm. In fact, all of the graphs in WWII for soot-containing snow are labeled with soot amounts that are probably a factor of 2 too large. This was due to an overestimate of soot density, which was pointed out in footnote 3 of WWII (see also *Roessler and Faxvog* [1979]). Figure 6 of this review is taken from WWII but with the soot amounts now altered to the more likely values.) The remaining discrepancy may be due to five causes.

1. The new accurate laboratory measurements of m_{im} by *Grenfell and Perovich* [1981] differ somewhat from the values of *Sauberer* [1950] used by WWI and WWII. Their use causes no difference in the maximum albedo value (although its position is at 0.46 μm rather than 0.40 μm) but causes a rise of ~0.01 in albedo at 0.9 μm.

2. Agreement between measurement and calculation can be further improved by speculating that grain size increases with depth (which was observed in one case).

3. Soot which is reported as an average concentration in the snow may actually be concentrated at the surface (which was also observed in one case) where it has more effect on albedo.

4. The measurement of soot concentration may have been in error. Grenfell et al. estimated an uncertainty of a factor of 2–3 in soot concentration.

5. There may be an incorrect assumption in the modeling. The calculations assumed that both soot particles and ice particles were surrounded by air. The possible location of soot particles inside the ice grains might enhance their absorption of light. However, it has not been demonstrated that a significant fraction of the soot could be inside the ice grains. Soot could be located inside a snow particle if it were attached to a dust particle which served as an ice nucleus. But it seems unlikely that soot collected by scavenging or dry fallout would end up inside ice grains.

2. *Volcanic Ash*

Volcanic ash currently seems to affect snow albedo only locally, but at times in the past it has probably reduced the albedo of the entire Antarctic continent (*Gow and Williamson* [1971], reviewed by WWII).

The most common magma is basalt, and the most common volcanic ash is andesite (R. Cadle, personal communication, 1980). Both of these rocks have very similar optical properties for short waves: $m_{im} \approx 1 \times 10^{-3}$, constant across the visible spectrum [*Pollack et al.*, 1973]. Thus their effect on snow albedo is qualitatively similar to that of soot, that is, giving no color to the snow; but in order to mimic a given concentration of soot, the andesite concentration must be 200 times higher.

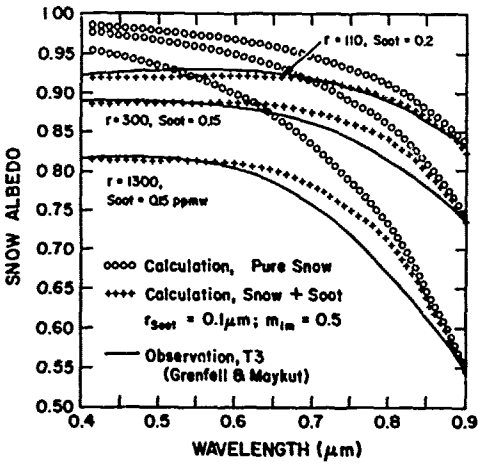

Fig. 6. Comparison of calculated snow albedo with observations at visible wavelengths. Solid lines are measurements of *Grenfell and Maykut* [1977, Figure 1] made in summer 1974 at ice island T-3 in the Arctic Ocean. In order of decreasing albedo they are (1) dry, cold snow, wind packed, deep drift, $\rho = 0.4$ g/cm^3, (2) 5-cm wet new snow over multiyear white ice, and (3) old melting snow, 28 cm thick. Circles are calculated albedo of semi-infinite pure snow for diffuse illumination, with grain radii to match observations at $\lambda = 0.9$ μm. In order of decreasing albedo they are (1) $r = 110$ μm, (2) $r = 300$ μm, and (3) $r = 1300$ μm. Plus signs are for snow containing the specified concentrations of soot, using for the imaginary index of refraction m_{im} (soot) = 0.5 independent of wavelength; $m_{re} = 1.8$. (Taken from Figure 6*b* of WWII but with soot amounts corrected according to footnote 3 of WWII).

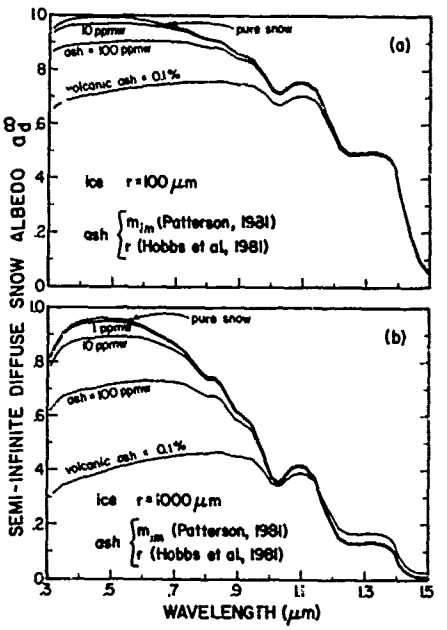

Fig. 7. Effect of Mount St. Helens ash on snow albedo for diffuse incidence: (*a*) snow grain size $r = 100$ μm; (*b*) $r = 1000$ μm. Ash parameters are described in the text.

For this review article we have done a special calculation of the effect on snow albedo of Mount St. Helens ash (Figure 7), using the model of WWII, for diffuse incident radiation. The ash particle size distribution is taken to be that measured from aircraft at 3200-m elevation, 130 km downwind of the volcano on May 19, 1980 [*Hobbs et al.*, 1981, Figure 2*c*]. This size distribution has about the same effect on snow albedo as does a uniform size of $r = 5$ μm. The real refractive index is taken as that of andesite ($m_{re} = 1.47$) from *Pollack et al.* [1973]. The imaginary index m_{im} (λ) was measured by *Patterson* [1981] for $0.3 \le \lambda \le 0.7$ μm. We take the values he gives for the ash which fell at Bozeman, Montana, and then interpolate from his value at 0.7 μm to the value for andesite at 1.2 μm. For $\lambda > 1.2$ μm we use the andesite values reported by Pollack et al. In the visible wavelengths the Mount St. Helens ash is measured to be more absorptive ($m_{im} \approx 4 \times 10^{-3}$) than was the andesite sample of Pollack et al. ($m_{im} \approx 1 \times 10^{-3}$) and also to be slightly reddish colored rather than perfectly grey.

The snow albedo in Figure 7 is reduced for $\lambda < 1$ μm by addition of ash. At longer wavelengths the albedo is unaffected unless the ash content exceeds 0.1%, in which case the albedo is increased for $\lambda > 1.15$ μm.

The eruption of Mount St. Helens has provided an opportunity to study the effects of volcanic ash on snowmelt. A curious puzzle reported by R. Armstrong (personal communication, 1980) is that although the melting rate on Mount Olympus in summer 1980 was enhanced by the Mount St. Helens ash, the formation of suncups [*Post and LaChapelle*, 1971, pp. 71–73] was dramatically inhibited. The solution to this puzzle may lead to further insight into the nature of the snowmelt process.

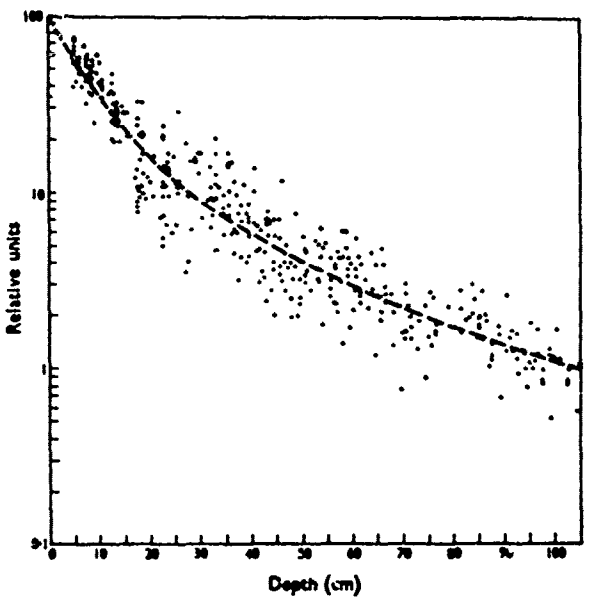

Fig. 8. Measurements of the downward flux of solar radiation in the snow at Plateau Station, Antarctica. The horizontal axis is geometric depth, not liquid-equivalent depth. (Figure 1 of *Schwerdtfeger and Weller* [1977].)

I. TRANSMISSION OF LIGHT THROUGH SNOW

1. *Spectrally Integrated Flux Extinction*

Figure 8, taken from *Schwerdtfeger and Weller* [1977] shows the extinction of all-wave solar radiation flux in clean, dry snow (ρ_s = 0.3 g cm^{-3}) of the Antarctic Plateau. The extinction is due to both scattering and absorption. It does not follow an exponential decay in the top 40 cm or so because the spectral composition of the downflux changes rapidly in this region. Only the visible radiation penetrates deeply. At a depth of 100 cm (30 cm liquid equivalent), 1% of the incident downflux remains unextinguished. This 1% is probably entirely blue light, concentrated in a narrow wavelength band about λ = 0.46 μm, where κ_i reaches its minimum.

The absorption of solar radiation is greatest near the surface and is due almost entirely to near-IR radiation [*Wiscombe and Warren*, 1980*b*, Figure 3] because most of the visible light eventually reemerges after multiple scatterings. *Choudhury* [1981, Figure 14] has calculated the solar flux divergence and the associated heating rates in the snow using an atmospheric radiation model coupled to his snow albedo model. He finds the heating rate at the surface to be about 20 times that at 5-mm depth for r = 300 μm but dependent on grain size. The factor is larger for smaller grains because radiation is attenuated more rapidly in fine-grained snow.

These calculated solar heating rates will, of course, be compensated by infrared cooling rates. The κ_s for thermal IR radiation is much larger than that for near-IR radiation, so the cooling is more concentrated at the surface than is the heating. This leads to the observation of temperature maxima at some depth below the surface in polar snowfields during the sunlit seasons. The temperature maximum at Pionerskaya (Antarctica) in December was located 8 cm below the surface [*Schlatter*, 1972, Figure 2]. Similar results are found in Greenland (W. Bow, personal communication, 1981). The depth of maximum net heating rate should vary with solar zenith angle, approaching the surface as $\theta_0 \rightarrow 90°$.

2. *Spectral Flux Extinction*

For the testing of theoretical models, monochromatic flux extinction measurements are more useful than the spectrally integrated measurements of Figure 8 because of the changing spectral composition with depth and the uncertain spectral composition of the incident sunlight.

Flux extinction measurements are more difficult to do accurately than are albedo measurements for diffuse incidence. (Albedo measurements under clear sky are also subject to error, as is explained in section J below.) The presence of the radiometer in the snowpack disturbs the radiation field more than it does above the snowpack; this disturbance was analyzed by *Giddings and LaChapelle* [1961]. A second difficulty which is more severe for extinction measurements than for albedo is 'leakage,' the detection of unwanted light from the wings of the filter function (T. C. Grenfell, personal communication, 1979). Leakage is least important at the wavelength of smallest absorption, λ = 0.47 μm. For example, one may nominally be measuring radiation flux at λ_1 because the filter function is centered at λ_1, but some small fraction of the light at λ_2 in the wing of the filter function also enters the detector. Unfortunately, the downflux at λ_2 deep in the snowpack may be orders of magnitude larger than that at λ_1, so that most of the light one reports at λ_1 was actually light of the wrong wavelength. This is a problem for extinction measurements but not for albedo measurements: for example, whereas the ratio of blue albedo (λ = 0.46 μm) to red albedo (λ = 0.7 μm) may be close to 1.0 (see Figure 1), the ratio of blue downflux to red downflux (for r = 110 μm in Figure 9*a*) may be ~60 at a depth of 10 cm (liquid equivalent) and ~4000 at 20 cm.

Figure 9 compares measurements with calculations of κ_s (λ). *Liljequist* [1956] used four filters to study the visible spectrum in Antarctic snow whose grain size he measured as r = 150 μm. *Kuhn and Siogas'* [1978] (hereafter KS) measurements in south polar snow probably had good spectral resolution throughout the range, whereas *Grenfell and Maykut*'s [1977] (hereafter GM) spectral resolution became poorer with increasing wavelength. Deconvolution was used for the longer wavelengths in an attempt to improve the resolution (T. C. Grenfell, personal communication, 1981). The data of GM in Figure 9 are probably reliable for $\lambda < 0.6$ μm.

Albedo had also been measured for these snow samples, and grain size was obtained by WWI and WWII by matching the calculated and observed albedo at $\lambda \geq 0.9$ μm, where impurities have negligible effect on albedo. (This was done for the albedos of KS and GM; Liljequist's albedos indicate that the snow at Maudheim was uncontaminated.) The grain sizes thus obtained (Figure 6) were r = 1300 μm for GM's old melting snow and $r \approx$ 110 μm for both GM's 'dry compact snow' and KS's south polar snow (r = 110 μm also tolerably matches Liljequist's albedos).

The model parameters necessary to explain the albedo agreed with the parameters necessary to explain κ_s only for Liljequist's measurements. (However, his measurements are unreliable for $\lambda \geq 0.6$ μm because of leakage as described above.) The presence of 0.5 ppmw of soot was found

necessary by WWII (after taking into account footnotes 3 and 4 of WWII) to explain the KS albedo measurements, yet Figure 9*a* shows that KS's flux extinction measurements are characteristic of pure snow, as can also be seen in Figure 11 of *Choudhury* [1981].

The calculations (circles and plus signs) in Figure 9 correspond to the circles and plus signs in Figure 6; the plus signs give κ_s for the soot amount necessary to explain the albedos of GM. Considering only $\lambda < 0.6$ μm for reasons mentioned above, the measured κ_s falls between the pure-snow κ, and the sooty-snow κ_s. This might be explained if the soot concentration at the surface at T-3 had been higher than its subsurface concentration. This is possible if the soot was the result of combustion of heating fuel, because the nearby building had been unoccupied until shortly before the measurements were made (T. C. Grenfell, personal communication, 1981). However, this argument probably cannot explain the data of Kuhn and Siogas; it is difficult to see how soot could be concentrated at the surface 1 km from the South Pole Station, rather than uniformly distributed.

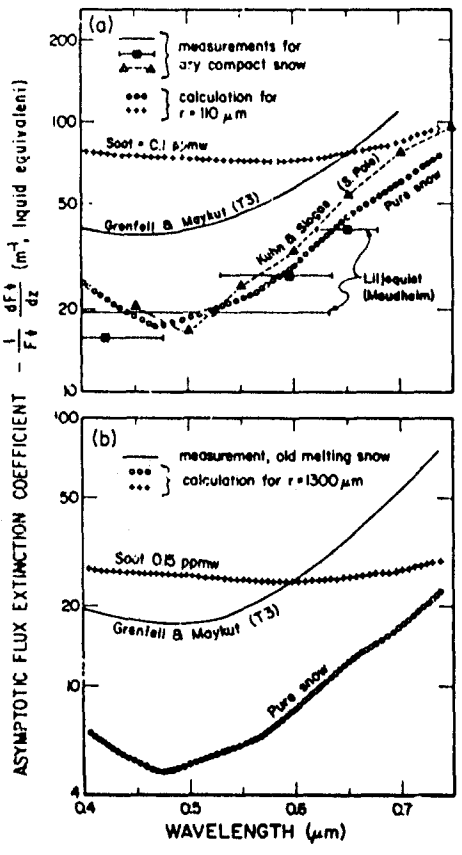

Fig. 9. Asymptotic flux extinction coefficient for snow as a function of wavelength in the visible spectrum. Solid lines are measurements of *Grenfell and Maykut* [1977, Figure 3]. Squares are Antarctic measurements of *Liljequist* [1956] for snow of measured grain size $r = 150$ μm. Bandwidths of Liljequist's filters are obtained from his Figure 48 and plotted here as the positions of half-maximum transmittance. Triangles are measurements of *Kuhn and Siogas* [1978] at South Pole Station. (All depth values have been converted here from snow depth to liquid-equivalent depth.) Circles are calculations using WWI model, with grain radii chosen to match albedo at $\lambda = 0.9$ μm for snowpacks shown in Figure 1 of *Grenfell and Maykut* [1977]. These are the same model snowpacks described by the top and bottom lines of the circles in Figure 6 of this paper. Plus signs are model calculations for snowpacks corresponding to the top and bottom lines of the plus signs in Figure 6.

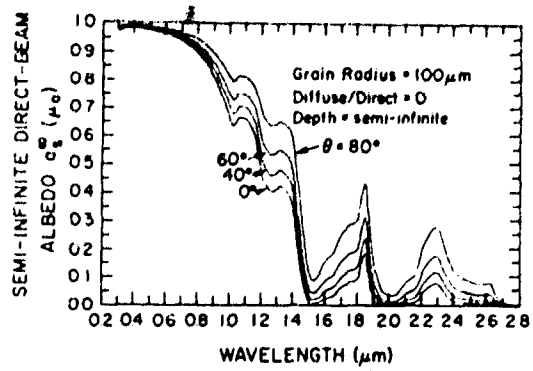

Fig. 10. Direct-beam albedo of a semi-infinite snowpack versus wavelength for several values of direct-beam zenith angle $\theta = \cos^{-1}\mu_0$. (Figure 11*a* of WWI. Reprinted by permission of the American Meteorological Society.)

These discrepancies indicate the need for more spectrally detailed measurements of both $\kappa_s(\lambda)$ and $a_s(\lambda)$ on the same snowpack. As *Choudhury* [1981] emphasized, a good theoretical model must explain both albedo and extinction measurements. With the currently available data we place more emphasis on explaining the albedo measurements than on explaining the κ_s measurements, because the latter are more susceptible to experimental error.

J. Dependence of Snow Albedo on Sun Angle

1. *Spectral Snow Albedo*

As is true for most surfaces, the albedo of snow increases as the sun nears the horizon. Figure 11*a* of WWI is reproduced here as Figure 10, showing model-calculated albedo for four zenith angles. The albedo is predicted to be sensitive to zenith angle in the near IR but not in the visible, in qualitative agreement with measurements of *Bryazgin and Koptev* [1969]. However, addition of trace amounts of impurities to the snow would allow a zenith angle dependence in the visible as well. (These calculations are for the extreme case of 100% direct-beam radiation. Even under clear sky the diffuse sky radiation would make the observed zenith angle dependence weaker than that shown in Figure 10.)

The reason that the albedo is higher for low sun is that a photon on average undergoes its first scattering event closer to the surface if it entered the snow at a grazing angle. If the scattering event sends it in an upward direction, its chance of escaping the snowpack without being absorbed is greater than it would be if it were scattered from deeper in the pack. This would be observed even if the ice particles scattered light equally in all directions. But the phenomenon is greatly enhanced by the extreme asymmetry of the scattering, whereby scattering within a few degrees of the forward direction is much more probable than scattering to other angles.

In all radiative transfer problems for a plane-parallel slab, as the direction of incidence goes toward grazing, the albedo becomes increasingly dominated by single scattering. As the sun goes down, the shoulder of the forward peak of the single scattering phase function begins to emerge more and more from the snowpack (Figure 11), whereas when the sun was higher it was buried because of its 5°–10° width. Naturally, it is the grains at the surface that are doing most of the scattering in this case. Figure 11 is purely schematic, be-

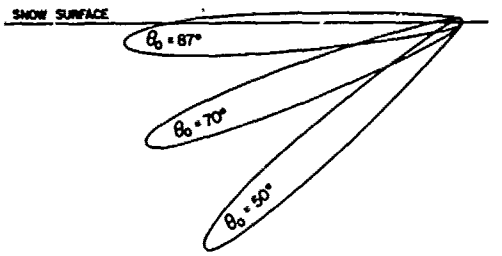

Fig. 11. Polar diagram of the scattering phase function of a snow particle at the surface of the snowpack for three solar zenith angles. This shows the probability that a scattered photon will go into any particular direction. For display purposes this phase function was calculated for an unrealistically small snow grain size ($r = 10$ μm, $\lambda = 5$ μm). The asymmetry of the phase function becomes much more extreme as r increases or λ decreases.

cause it was calculated for spherical ice particles. For hexagonal columns or plates the 22° halo may contain as much energy as the forward peak [*Wendling et al.*, 1979, Figure 5], and this halo begins to emerge from the snowpack already at $\theta_0 \approx 65°$.

With very low sun we approach a pure single-scattering situation, so that the bidirectional reflectance becomes just the single-scattering phase function.

At the same time the assumption of sphericity of snow grains breaks down. The effects of angular details are smeared out with multiple scattering, so that the grains can be treated as spheres. But the angular effects become dominant as $\theta_0 \to 90°$.

Besides the breakdown of the sphericity assumptions as $\theta_0 \to 90°$, the delta-Eddington approximation also becomes poor, for reasons which are given by *Wiscombe* [1977]. The disagreement between model and observation as $\theta_0 \to 90°$ is attributed (below) to this breakdown of delta-Eddington approximation.

All of this can be discussed in terms of standard single-scattering and multiple-scattering theory. There is no need to invoke a separate 'surface reflection.' Specular reflection is an acceptable natural part of the single-scattering pattern of hexagonal plates and prisms and other ice crystal forms. Hence if one would use a fully correct single-scattering phase function instead of the spherical Mie phase function, and an exact radiative transfer method for multiple scattering, one could properly model the albedo as $\theta_0 \to 90°$.

There are no nomochromatic measurements against which to test the model. This is unfortunate, because the discrepancies in spectrally integrated albedo between model and observation described below might be pinned down if measurements would be made at discrete wavelengths.

2. *Spectrally Integrated Snow Albedo* $\bar{a}$ (μ_0)

This is a controversial subject at present. The reasons for the confusion are (1) modeling error, (2) instrument error, (3) inadequate observation of snow grain size, impurity content, and surface roughness, all of which should affect the slope of $\bar{a}(\mu_0)$, and (4) inadequate knowledge of the spectral distribution of the incident radiation.

A number of clear-sky measurements of spectrally integrated snow albedo as a function of the cosine μ_0 of the solar zenith angle θ_0 are plotted in Figure 12, along with model results. (The only reason for plotting the data on the two separate frames (Figures 12*a* and 12*b*) is to avoid clutter.) Considering first Figure 12*a*, we note that the model calculations of *Wiscombe and Warren* [1980*b*] (for the atmospheric conditions of the Antarctic Plateau and $r = 100$ μm) show a much weaker dependence of $\bar{a}$ on μ_0 than do the observations by *Hubley* [1955] on the Juneau Icefield, *Korff et al.* [1974] in Colorado, and *Rusin* [1961] in Antarctica. (Note that the model does not account for the sphericity of the atmosphere, which probably makes it unreliable for $\mu_0 < 0.1$ or so.)

The responses of all commercial radiometers deviate from a proper 'cosine law' [*Liljequist*, 1956; *Dirmhirn and Eaton*, 1975]. They are usually less sensitive at large incident zenith angles. If not corrected for, this causes albedos at low sun to be overestimated. This is because the reflected radiation is more diffuse than the incident radiation. The steep dependence of $\bar{a}$ on μ_0 reported by Rusin and by Hubley might be explained as this type of error. But the measurements of Korff et al. must be considered reliable because they calibrated their instrument and applied a correction at large zenith angles.

Hubley's results show an interesting hysteresis, with higher albedo in the morning than afternoon at the same zenith angle. Hubley speculated that this might be attributed to specular reflection from firnspiegel in the morning before the melting began.

In Figure 12*b* are plotted several Antarctic measurements and calculations. *Carroll and Fitch*'s [1981] (hereafter CF) measurements extended to larger zenith angles than anyone else has reported and show a much steeper dependence of $\bar{a}$ on μ_0 than *Liljequist* [1956] found. Liljequist's instruments had been extensively calibrated for the dependence of their response on both the zenith and the azimuth solar angles [*Liljequist*, 1956, pp. 45–55]. CF did not report such calibrations for their instrument, so it is possible that their dramatic disagreement with Liljequist is at least partly caused by an experimental bias in CF's measurements.

CF's measurements were complicated by surface irregularity. The faces of oriented sastrugi present different angles to the sun as it moves around the horizon. Accordingly, CF noted a diurnal cycle of albedo, as had *Kuhn and Siogas* [1978], with higher values when the sun was oriented parallel to the sastrugi, so that the effective zenith angle was larger. The measurements of CF plotted in Figure 12*b* are the averages of four solar azimuths 6 hours apart. A representative error bar is drawn on one of the points.

There are actually several effects of surface roughness on albedo. In a field of randomly oriented surface roughness features (or in the daily average at the south pole) when the sun is low, the effective zenith angle is always smaller for a rough surface than for a flat surface (section 5*c* of WWI). This means that CF's observed dependence of $\bar{a}$ on μ_0 would be even steeper if μ_0 were taken as the effective value instead of the flat surface value, and their results would deviate even more dramatically from the results of other experimenters plotted in Figure 12.

However, this is further complicated by the fact that the effective zenith angle is a function of wavelength. In order for surface roughness to moderate the zenith angle effect its typical length and depth must not be much smaller than the average penetration depth of light into snow. Surface irregu-

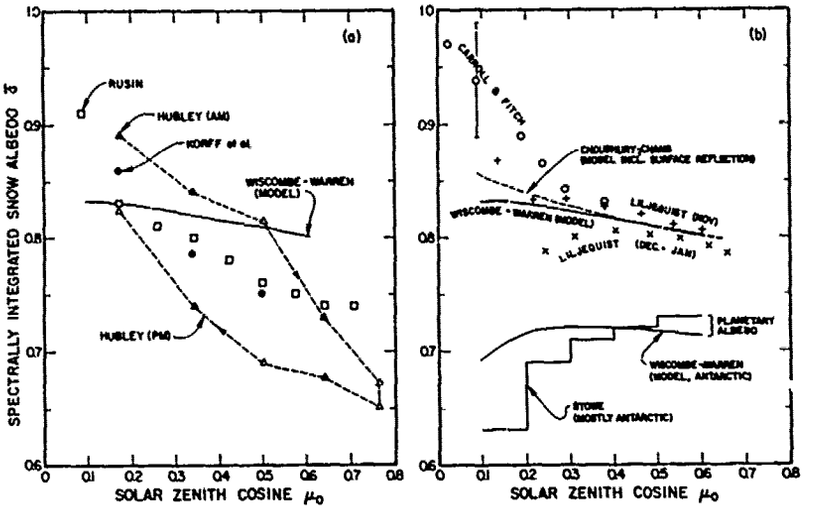

Fig. 12. Spectrally integrated clear-sky snow albedo as a function of μ_0 according to various investigators. The result of the *Wiscombe and Warren* [1980*b*] Antarctic model is plotted in both frames for reference. The lower two plots in Figure 12*b* are for Antarctic planetary albedo.

larities on smaller scales are less important because a significant amount of radiation penetrates right through a peak and emerges on the other side. Thus whereas surface roughness of millimeter scale affects the reflection of visible light by soil particles, it does not affect the reflection of visible light by snow.

Besides altering the effective zenith angle, surface roughness will also decrease the albedo further by trapping some radiation in the troughs, as described in section E5*b*.

In addition to these systematic effects there is a sampling error which arises in albedo measurements of a rough surface. One should ideally make measurements from high towers [*Langleben*, 1968] so as to get a representative view of the surface. Close to the ground the field of view may contain only one or a few sastrugi and will thus contain more or less than its fair share of shadow, depending on solar azimuth.

The delta-Eddington snow albedo model of WWI was coupled to the atmospheric radiation model of Wiscombe for cloud-free January conditions of the Antarctic Plateau [*Wiscombe and Warren*, 1980*b*]. The zenith angle dependences of both surface albedo and planetary albedo are shown in Figure 12*b*. The model adequately explains the $\bar{\alpha}(\mu_0)$ observed by *Liljequist* [1956] but clearly fails to reproduce that of CF. (The reduction of December-January albedo at large zenith angles which shows up in Liljequist's daily averages was only observed in the afternoon and was attributed by Liljequist to metamorphism rather than to zenith angle. This is a possible complicating factor in all of these studies.)

Choudhury and Chang [1981] added 'surface reflection' to their model, as described in section E4 above, in order better to match the November measurements of Liljequist. But in order to get even this slight steepening of the $\bar{\alpha}(\mu_0)$ shown in Figure 12*b* they had to use what seems an unreasonably small slope variance $s^2 = 0.01$, which would be more appropriate for a glazed crust than for the dry snow grains of Antarctica. The point we wish to emphasize here is that the addition of even this extreme amount of surface reflection is dramatically inadequate to bring the delta-Eddington model in line with CF's observations. If these observations must be matched instead of those of Liljequist, a problem with the delta-Eddington model is indicated that cannot be corrected by adding an ad hoc surface reflection.

Delta-Eddington is known to underestimate the albedo of a plane-parallel layer at large zenith angles. It agrees very well with the exact doubling calculations [see *Joseph et al.*, 1976, Figure 3] for $\mu_0 \geq 0.4$ ($\theta_0 \leq 66°$), but albedo errors of up to 10% can occur at $\mu_0 = 0.1$ ($\theta_0 = 84°$) for particular values of g and $\tilde{\omega}$. In order to quantify the errors of the delta-Eddington method for snow at low sun, it will be necessary to do some albedo calculations which give a more exact account of the radiative transfer process.

3. *Spectrally Integrated Planetary Albedo*

Model calculations of spectrally integrated planetary albedo over the Antarctic Plateau plotted in the lower part of Figure 12*b* show planetary albedo to increase slightly from $\mu_0 = 0.6$ to $\mu_0 = 0.3$ because of the μ_0 dependence of surface albedo. But when the sun goes even lower, a second effect comes into play to reduce the albedo. This is the increased H_2O and O_3 absorption in the atmosphere due to the longer slant path of the sunlight.

The zenith angle dependence of planetary albedo of the snow-atmosphere system is being measured by *Stowe et al.* [1980, personal communication, 1980] using the scanning radiometer of the Nimbus 7 satellite. For that work all snow-covered scenes at the same zenith angle are considered equivalent, regardles of geographic location. However, for the 1 month of data available so far (November 1978), nearly all of the scenes were over Antarctica. These observations of Stowe et al. plotted as the histogram in Figure 12*b* show a steeper decrease in albedo as μ_0 decreases. It is probably premature to comment on the differences between Stowe's observations and the model predictions, since many factors remain to be considered, but it is noteworthy that both model and observation agree on a range of about 70–73% for

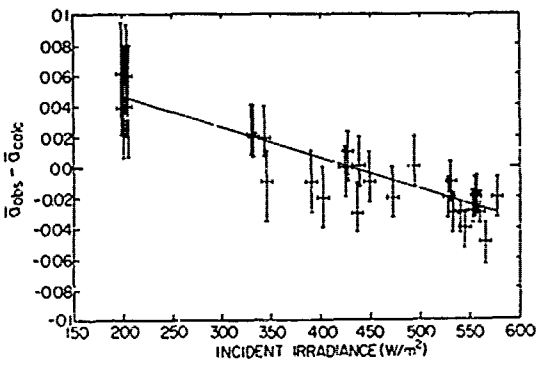

Fig. 13. Effect of cloud cover on spectrally integrated snow albedo. The difference between observed and calculated spectrally integrated albedos is plotted versus incident irradiance (which is here approximately proportional to atmospheric transmissivity, because the measurements were all made between 1100 and 1400) for snow in the Cascade Mountains. 'Calculated' albedos were calculated by *Grenfell et al.* [1981] using observed spectral albedos with a fixed incident spectral distribution characteristic of an intermediate cloud thickness. The straight line is a least squares fit to the data points. (Figure 5 of *Grenfell et al.* [1981]. Reprinted by permission of Elsevier.)

$\mu_0 \geq 0.2$. Of all the surface types examined by Stowe et al., snow was the only one in which the atmospheric path length effect was able to dominate over the surface albedo effect. In order to be consistent with these planetary albedos, the μ_0 dependence of the snow surface albedo would have to be even smaller than the modest dependence given by the delta-Eddington model.

In summary, (1) the delta-Eddington method underestimates albedo at low sun (the magnitude of this underestimate could be determined by doing a more exact calculation), and (2) the Antarctic planetary albedo measurements of Stowe et al. and the Antarctic surface albedo measurements of Carroll and Fitch are mutually inconsistent.

Our detailed discussion here of extreme zenith angles ($\theta_0 \rightarrow 90°$) is important for focusing on discrepancies between model and observation, but it has very limited relevance for the snow energy budget. Even at the north and south poles, only 3% of the annual irradiance is received at $\mu_0 < 0.1$ ($\theta_0 > 84.3°$), and only 13% at $\mu_0 < 0.2$ ($\theta_0 > 78.5°$). At other latitudes these percentages are even smaller.

K. Effects of Cloud Cover on Snow Albedo

1. *Monochromatic Albedo*

The only effect of cloud cover on monochromatic albedo is to diffuse the radiation, changing the effective zenith angle. The effective zenith angle for purely diffuse radiation is about 50°. Thus as shown in Figure 12 of WWI, the interposition of a cloud layer between sun and snow causes spectral snow albedo to increase for $\theta_0 < 50°$ and to decrease for $\theta_0 > 50°$, the latter being the normal situation over snow-covered surfaces.

2. *Spectrally Integrated Albedo*

Cloud cover is normally observed to cause an increase in spectrally integrated snow albedo. This is because clouds absorb the same near-infrared radiation that snow would absorb, leaving the shorter wavelengths (for which snow albedo is higher (cf. Figure 1)) to penetrate to the surface. This was pointed out by *Liljequist* [1956, p. 88], *Grenfell and Maykut* [1977, p. 457], and WWI (section 5*d*). This 'spectral shift' effect (named by CF) dominates the contrary 'zenith angle alteration' effect discussed above but is moderated by it, as seen in Table 173 of *Rusin* [1961].

An example of the spectral shift effect is shown in Figure 13, which is taken from *Grenfell et al.* [1981]. The difference $\bar{a}_{obs} - \bar{a}_{calc}$ is plotted, where $\bar{a}_{calc}$ was based on the spectral albedo measurements and was calculated by Grenfell et al. assuming a fixed spectral distribution of incident radiation characteristic of an intermediate cloud thickness. Under a thick overcast the albedo is found to be 1–9% higher than it would have been under an intermediate cloud condition.

An interesting exception to the general rule that snow albedo is higher under cloud cover has been reported by CF to occur at very low sun and can be directly traced to the much steeper dependence of $\bar{a}$ on μ_0 that they found at these sun angles (Figure 12*b*). At the low solar elevations encounterd by CF at the south pole, the change in effective zenith angle caused by clouds is apparently more than able to compensate for the spectral shift effect.

L. Bidirectional Reflectance of Snow

1. *Complete Description (for Satellite Measurements)*

The radiation reflected by a snow surface is not distributed uniformly into all angles. If it were, then the principle of reciprocity [*Siegel and Howell*, 1972] would indicate that snow albedo was independent of θ_0. The pattern of reflection is described by the anisotropic reflectance function f, which depends on the source zenith angle θ_0, detector nadir angle θ', and the relative azimuth $\phi' - \phi_0$. The bidirectional reflectance R is the product of the albedo and f, as given by equation (1). If the surface conditions depend on azimuth, as is the case for the oriented sastrugi at the south pole, f is actually a function of the two individual azimuth angles ϕ_0 and ϕ' rather than merely of their difference, but this complication is usually ignored; f may also depend on snow grain size and snow depth.

Satellite detectors with narrow fields of view measure R at only one or a few angles. In order to obtain the planetary albedo from individual satellite measurements it is thus necessary to have prior knowledge of f. Measurements of f have been made at the surface by *Middleton and Mungall* [1952] and *Dirmhirn and Eaton* [1975], from low-flying aircraft by *Griggs and Marggraf* [1967] and *Salomonson and Marlatt* [1968*b*] (with more details by *Salomonson and Marlatt* [1968*a*]), and from satellite by *Stowe et al.* [1980, personal communication, 1980].

Because the single-scattering phase function varies with wavelength, f could additionally be a function of wavelength. However, *Griggs and Marggraf* [1967] have found f to be independent of λ, at least for $0.44 \leq \lambda \leq 0.96$ μm. If this holds also at longer wavelengths (which seems unlikely), it means that f can be obtained from spectrally integrated measurements.

Figure 14 shows the results of the two most comprehensive sets of measurements. (The other reports cited above included measurements at only a few angles.) *Dirmhirn and Eaton* [1975] measured f for a melting snowpack five times (i.e., at five sun angles) on a single afternoon in Utah. (They reported that snow appeared glazed at sunrise and sunset,

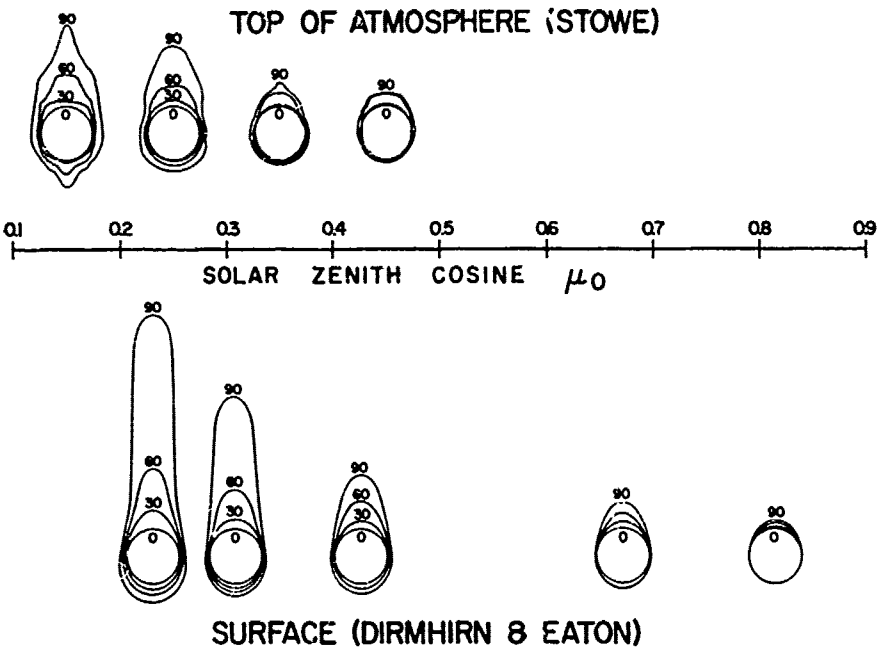

Fig. 14. Anisotropic reflectance functions for snow at the surface [from *Dirmhirn and Eaton*, 1975, Figure 3] and at the top of the atmosphere (replotted from data of *Stowe et al.* [1980, personal communication, 1980]).

but since it was melting in the afternoon when measurements were taken, we doubt that glazing affected the measurements.) A separate diagram is given for each solar zenith angle θ_0; at each θ_0, f was measured at eight azimuths $\phi' - \phi_0$ for four nadir angles θ': 0°, 30°, 60°, and 90°. In each diagram, f is proportional to the distance from the center of the inner circle to the appropriate point on the curves, but for use it must be normalized for each diagram so that

$$\frac{1}{\pi} \int \int_{\text{hemisphere}} f(\mu_0, \mu', \phi' - \phi_0)\, \mu'\, d\mu'\, d\phi' = 1 \quad (4)$$

The solar beam is taken to be incident from below. There is enhanced reflectance in the forward direction, and the anisotropy increases as μ_0 decreases (i.e., as the sun goes down).

Stowe et al. [1980] have taken scanner data from the Nimbus 7 satellite and grouped them into bins of $(\theta_0, \theta', \phi' - \phi_0)$. Since the satellite did not examine a single target at all angles, the measurements from all snow surfaces on earth were treated together and assumed to have the same f. However, at the time of this pilot experiment (November 1978) most of the earth's sunlit snow area was actually in the Antarctic, so the results of Stowe et al. (top of Figure 14) are really representative of a snow surface uncontaminated by vegetation. They show less anisotropy than do the measurements at the surface. This difference may partly be due to the diffusing effect of the intervening atmosphere, but there may also be an actual difference in f between the two snow types (dry, clean, fine-grained Antarctic snow versus old, melting, somewhat glazed mid-latitude snow). These results were from only a small sample of the satellite data and will be augmented in the future.

The bidirectional reflectance of snow has not been modeled since the work of *Barkstrom and Querfeld* [1975] reviewed in section E2 above. The doubling [*Hansen*, 1969] or discrete ordinates [*Stamnes and Swanson*, 1981] radiative transfer solutions would be useful in this connection, although surface roughness may be as important as doing the plane-parallel radiative transfer correctly, because of its two effects discussed above: altering the effective zenith angle by putting some of the snow in shadow and trapping light by multiple reflections among troughs and peaks.

2. *Azimuthally Averaged Bidirectional Reflectance (for Flux Calculations)*

For radiation budget calculations which produce only fluxes and not intensities, the full BRDF is not needed. One only requires the albedo and the azimuthally averaged anisotropic reflectance factor $\bar{f}$:

$$\bar{f}(\theta_0, \theta') = \frac{1}{2\pi} \int_0^{2\pi} f(\theta_0, \theta', \phi' - \phi_0)\, d\phi'$$

S. G. Warren and W. J. Wiscombe (unpublished data, 1980) derived a parameterization for $\bar{f}$ from observations of snow reflectance. They then used it to apportion the model-calculated snow albedo among the reflection nadir angles θ'.

In Figure 15 are plotted values of $\bar{f}$ they obtained from azimuthal averaging of measurements of f from four reports. Each set of connected points corresponds to a particular zenith angle θ_0. A straight line was fit to each of these 10 plots:

$$\bar{f} = 1 + b(\mu' - 1) \quad (5)$$

(The data in Figure 15 have been normalized so that the least squares lines all pass through the point (1, 1).)

The slopes b of these lines are plotted versus the solar zenith cosine μ_0 in Figure 16. They show approximately a linear dependence on μ_0, so the resulting parameterization for $\bar{f}$ is

$$\bar{f}(\mu_0, \mu') = [3/(3 - b)][1 + b(\mu' - 1)] \quad (6)$$

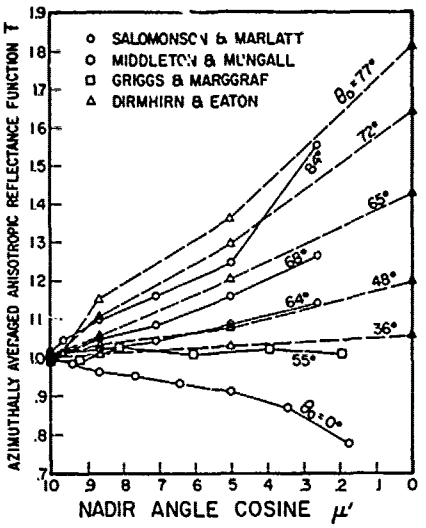

Fig. 15. Azimuthally averaged anisotropic reflectance function $\bar{f}$ of snow as a function of nadir angle cosine μ', scaled so that $\bar{f}(1) = 1.0$ for the least squares linear fit of each data set. The data points were obtained by azimuthally averaging charts published in four reports, as follows: *Salomonson and Marlatt* [1968*a*, *b*]: Measurements of f for snow (depth unspecified) in Utah and Wyoming from aircraft 120 m above the surface, wavelength channel 0.55–0.85 μm. Results were very similar for the 2- to 4-μm channel. *Middleton and Mungall* [1952]: Measurements at the surface using artificial incandescent lighting. Plotted here are results derived from their Figure 3*a* for wind-packed snow. The anisotropy exhibited by this snow sample was greater than for new snow fallen in calm. Observations were made only in the plane of incidence, so there are insufficient observations to do an azimuthal average for any zenith angles except $\theta_0 = 0°$, which is the case plotted here. *Dirmhirn and Eaton* [1975]: Measurements made at the surface under natural sunlight, April afternoon in Utah, melting snow. *Griggs and Marggraf* [1967, p. 153]: Measurements from aircraft, 120 m above the surface of a snow-covered lake, Oregon, snow depth of ≈1 m. Measurements were made at coarse azimuthal resolution ($\Delta\phi = 60°$) but at eight discrete wavelengths between 0.44 and 0.96 μm; f appeared to be independent of wavelength.

where $b = 1.07\mu_0 - 0.84$. The prefix $3/(3 - b)$ is a normalizing factor, chosen so that (4) is satisfied. The dependences of f on μ_0 and μ' are different, so (6) does not satisfy the reciprocity principle and is only a first attempt to parameterize available data.

The measurements used to obtain (6) were made under a variety of snow conditions with unspecified grain size, and it is likely that (6) is not really correct for all wavelengths and grain sizes. However, *Wiscombe and Warren* [1980*b*] found that their radiant flux calculations were actually insensitive to the functional form of $\bar{f}$; they obtained almost identical fluxes whether they used (6) or, alternatively, assumed isotropic reflectance. The largest differences in fluxes at the surface occurred in the visible wavelengths and were at most 0.6%.

M. Thermal Infrared Emission From Snow

1. *Emissivity*

We have taken many pages to discuss the solar reflectance of snow, yet its infrared emission deserves only a few paragraphs. The reason for this is that the infrared emissivity of snow is quite insensitive to snowpack parameters. For many purposes one can simply assume a snow emissivity of about 99%, as was measured by *Griggs* [1968].

Berger [1979] adapted the derivations of *Bohren and Barkstrom* [1974] to the limit of large absorption as described in section E2 above. His calculated emissivity (Figure 17) is independent of grain size but decreases slightly with increasing density. This calculated density dependence may depend on the particular regular array of spheres assumed by Berger, as noted above.

The albedo model of WWI was used to calculate emissivity (Figures 8*b* and 11*b* of WWI) by virtue of Kirchhoff's law [*Siegel and Howell*, 1972, p. 70]:

$$\varepsilon(\theta_0, \lambda) = 1 - a_s(\theta_0, \lambda)$$

where a_s is the albedo for zenith angle θ_0 and ε is the directional thermal emissivity at the same wavelength into the viewing (nadir) angle θ_0. Figure 18 shows the calculated dependence of snow emissivity on wavelength, averaged over emission angle for five grain sizes (Figure 18*a*) and for a single grain size $r = 100$ μm at four emission angles (Figure 18*b*). Since these calculations were done without a near-field correction, we do not show results beyond 40-μm wavelength, and the results plotted may already be somewhat inaccurate at $\lambda = 20$ μm, especially for $r = 50$ μm.

The emissivity is sensitive to grain size only at certain wavelengths. In particular, it is completely insensitive to grain size over most of the Planck function for normal terrestrial temperatures, centered near $\lambda = 10$ μm. The Mie results thus support *Berger*'s [1979] assumption of no transmission of IR radiation through ice spheres in this spectral range, which led to his prediction that emissivity would be independent of grain size.

The model of WWI does not compute a dependence of ε on ρ_s. However, because of the small penetration depth of thermal IR radiation in ice, 'surface roughness' on the scale of millimeters may affect emissivity. *Berger*'s [1979] dependence of ε on ρ_s is actually caused only by the relation he obtained between ρ_s and 'projected areas of surface and subsurface particles' (his equations 27 and 28), which seems actually to be a measure of surface roughness.

Because of the large m_{im} of ice throughout the thermal infrared, only a very thin layer of snow is already effectively

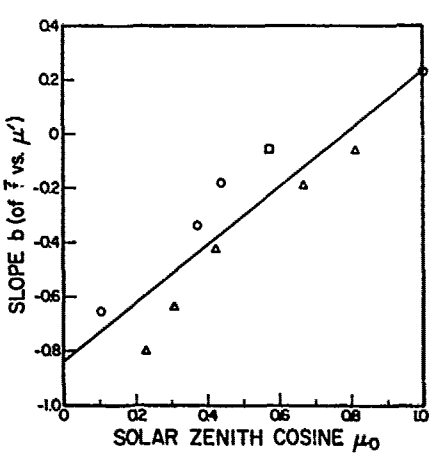

Fig. 16. Slopes (b in equation (5)) of the lines in Figure 15 are plotted here versus μ_0. The line is a least squares fit to the points. Symbols refer to the data sources given in Figure 15.

semi-infinite, so ε is independent of snow layer thickness. Small amounts of impurities will also not affect ε.

Figure 18*b* shows that the emissivity is near 100% for overhead viewing ($\theta_{out} = 0°$) but is significantly lower for large nadir angles. Thus the satellite viewing angle should be taken into account when inferring snow temperatures from satellite infrared channel ($\lambda \sim 11$ μm) emission measurements. The results in Figure 18 were obtained using the delta-Eddington approximation, so for $\theta_{out} = 80°$ the true emissivity may actually be lower than that shown.

2. *Brightness Temperature*

If $\varepsilon < 1$, the brightness temperature T_B at a single wavelength will be smaller than the true temperature T. The difference $T_B - T$ depends not only on ε but also on wavelength because of the variation of the Planck function with wavelength. J. Dozier (personal communication, 1981) has calculated $T_B - T$ for $3 \leq \lambda \leq 14$ μm for snow near the melting temperature, plotted in Figure 19. The assumption that snow is a blackbody could lead to an underestimate of temperature by as much as 2.5 K at $\lambda = 14$ μm and $\theta' = 75°$. However, the estimation of snow temperature from satellites will likely be subject to more error from uncertainty in atmospheric transmissivity than from uncertainty in snow emissivity.

N. REMOTE SENSING OF SNOW

1. *Snowpack Properties From Albedo Measurements*

Dozier et al. [1981] have used the model of WWI to calculate snow albedos integrated over channels 1 and 2 of the NOAA Tiros N satellite (0.5–0.7 μm and 0.7–1.0 μm, respectively). The hope is to deduce grain size from a near-IR channel, where depth and contaminants have no effect on albedo, and then use the deduced grain size together with the channel 1 data to infer snow water equivalent depth below some threshold value around 100 mm. Among the difficulties in this approach are (1) the conversion of bidirectional reflectance to albedo, (2) the poor location of channel 2 for this purpose (an ideal channel would be located in the region 1.0–1.2 μm, where the sensitivity of albedo to grain size is greatest), and (3) the fact that visible albedo reduction can be due to impurities as well as to thinning of the snowpack.

Dozier et al. were apparently able to detect the thinning of the snowpack at the end of the melting season on some Canadian lakes. Figure 20 is taken from their work. On the earlier date, April 12, the snow-covered lakes are brighter than the intervening forest in both channels. Two weeks later, much of the snow had melted, so that on April 27 there was less contrast in both channels between lake and forest. On both of these dates it is apparent that for snow the near-IR reflectance is smaller than the visible reflectance, in agreement with Figure 1. The forest exhibits the opposite behavior, in agreement with the known spectral reflectance of green plants [*Gates*, 1980]. Hopefully, in the future this work will be combined with ground truth measurements of snow depth.

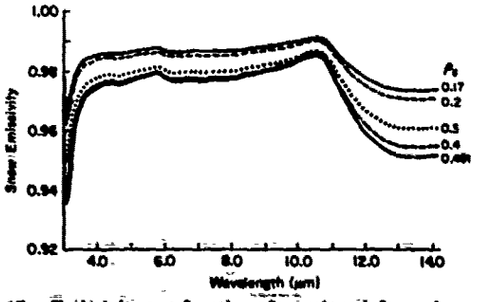

Fig. 17. Emissivity as a function of wavelength for various snow densities, according to the model of *Berger* [1979]. (Figure 7 of *Berger* [1979].)

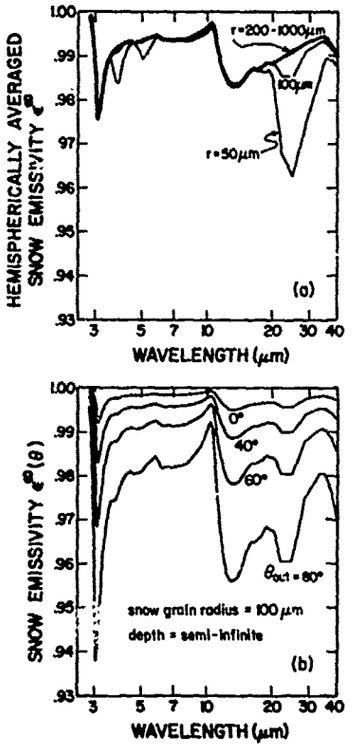

Fig. 18. Thermal infrared emissivity of snow as a function of wavelength, according to the model of WWI. (*a*) Hemispherically averaged emissivity for snow grain sizes r = 50, 100, 200, 500, 1000 μm. (*b*) Directional emissivity for four detector nadir angles.

Some experiments at the surface which are relevant to this problem are being done by *O'Brien and Koh* [1981]. They observed the change in spectral reflectance (using a few narrow-band filters) as a thick snow cover decayed, documenting the transition from the spectral reflectance of snow to the spectral reflectance of grass. As is expected (Figure 13 of WWI), the underlying surface first begins to 'show through' in the visible wavelengths and is evident in the near IR only when the snow cover is much thinner. Because of the somewhat crude experimental setup, these results are as yet only qualitative.

Detection of the dust content of snow has been attempted by *Sydor et al.* [1979] for polluted snow in Duluth harbor. However, dust was reported as rates of deposition rather than as weight fractions in snow, so no direct comparison with a model can be made.

Matson and Wiesnet [1981] describe the routine global mapping of snow cover using visible-channel imagery from

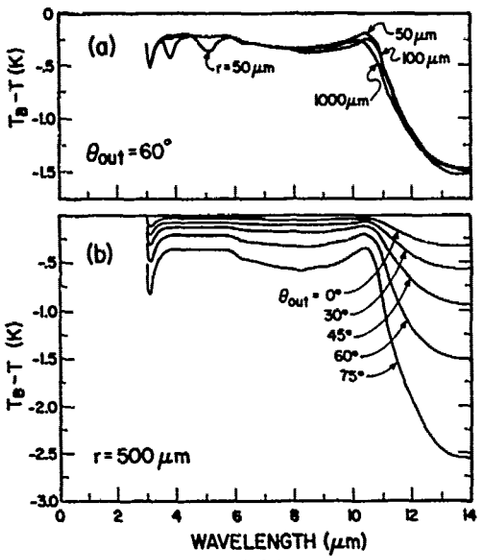

Fig. 19. Difference between brightness temperatures T_B and snow temperature T as a function of wavelength (*a*) for three different snow grain sizes at viewing angle $\theta' = 60°$ and (*b*) for snow grain radius $r = 500$ μm at five different viewing angles. Figure from J. Dozier (personal communication, 1981).

NOAA satellites. This monitoring program has been useful in describing the interannual variability of regional snow cover.

2. *Snow Cloud Discriminator (1.6 μm)*

Measurements from aircraft of spectral reflected intensity in the 1.4- 1.8-μm wavelength region have shown that clouds

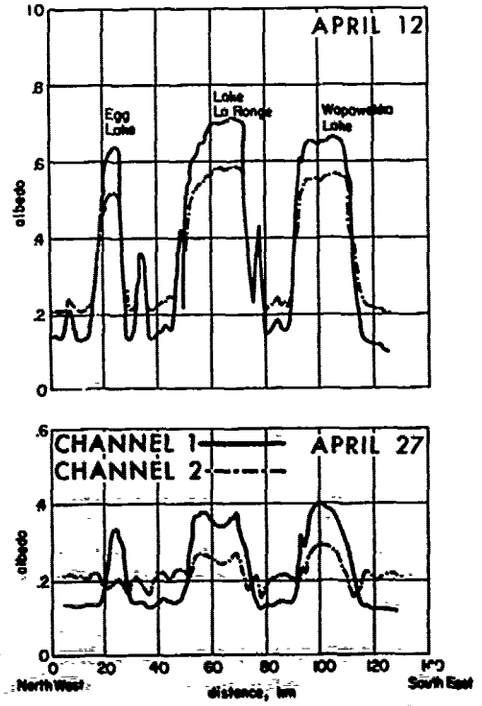

Fig. 20. Traces of reflectance measured from satellite by NOAA scanning radiometer across three lakes in Saskatchewan on two different days in visible channel 1 (0.5–0.7 μm) and near-IR channel 2 (0.7–1.0 μm). (Figure 10 of *Dozier et al.* [1981].)

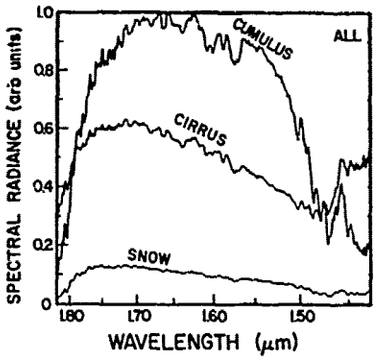

Fig. 21. Relative reflectance of snow and clouds as a function of wavelength from aircraft observations. (Figure 14 of *Valovcin* [1978].)

can be distinguished from snow. Figure 21 is taken from the report of *Valovcin* [1978]. The reflectance of cirrus clouds is shown to be greater than that of snow. This is because cirrus particles have a much smaller effective mean radius than do snow particles (perhaps 20 μm as opposed to 200 μm) and the albedo is higher for smaller ice grains (cf. Figure 1). The fact that cumulus clouds have even higher reflectance is due in part to each of three causes:

1. Cumulus clouds are thicker than cirrus.
2. Water is less absorptive than ice in this spectral region.
3. Cloud water droplets are smaller than cloud ice particles. (The cumulus clouds studied were all water droplet clouds, even at their tops.)

These aircraft observations have led to the employment of a 'snow cloud discriminator' channel at $\lambda = 1.6$ μm on a Defense Meteorological Satellite Program satellite. This channel cannot distinguish between thin cloud cover over bare ground and snow cover, but these can be distinguished in the visible channel; a bispectral method should therefore be quite reliable as a snow cloud discriminator. Tests of the utility of the 1.6-μm channel are under way by comparison with results from human analysis of satellite imagery, who use pattern recognition methods [*Woronicz*, 1981], or from ground-based observations of snow and cloud (R. Barry, personal communication, 1981).

3. *Thermal Infrared*

The temperature of a snowpack should be detectable from the thermal infrared emission, provided that the dependence of emissivity on viewing angle (Figure 18*b*) and the atmospheric transmissivity are accounted for.

4. *Summary of Snow Parameters Detectable in Solar, Infrared, and Microwave Spectra*

Table 2 offers a rough allocation of the snow parameters affecting solar spectral albedo, thermal infrared spectral emissivity, and microwave spectral emissivity. The microwave emissivity depends on three additional variables which are unimportant for the shorter waves: (1) liquid water content, because the m_{im} for ice and water are very different in the microwave; (2) temperature, because the m_{im} of ice (and of water) exhibits a significant temperature dependence for $\lambda \gtrsim 0.2$ mm; and (3) density, because snow grains are in each others' near fields at these wavelengths.

TABLE 2. Parameters Affecting Albedo and Emissivity of Snow

	Visible Solar Albedo	Near-IR Solar Albedo	Thermal Infrared Emissivity	Microwave Emissivity
Grain size	(+)	yes		yes
Zenith (or nadir) angle	(+)	yes	yes	yes
Depth	yes			yes
Contaminants	yes			
Liquid water content				yes
Density				yes
Temperature				yes

The sign (+) means only if snowpack is thin or impurities are present.

No attempt is made here to subdivide the microwave region. If that is done, one may find that the emissivity is insensitive to some of the parameters in Table 1 at certain wavelengths.

The thermal infrared emission can be used to obtain snow temperature. But a multiplicity of factors are seen to affect the optical properties of snow in other spectral regions. In order to detect individual snow parameters unambiguously from satellite, one must therefore examine the snow at several wavelengths simultaneously.

O. Recommendations for Modeling and Experimental Work

To test the theoretical radiative transfer models, more visible and near-IR measurements are needed of monochromatic flux extinction and of the zenith angle dependence of monochromatic albedo in situations where all relevant snow parameters (see Table 2) are measured simultaneously. The spectral emissivity in the thermal IR should be measured as a function of density and viewing angle. Reflectance measurements for unusual snow conditions would also be useful, such as snow covered with firnspiegel and rapidly melting snow which may have a high liquid water content. Special attention should be devoted to characterizing absorptive impurities in snow.

For remote sensing applications, angularly detailed measurements of the bidirectional reflectance for various wavelengths, grain sizes, and surface conditions should be given high priority.

Topics for future modeling include the study of near-field effects, nonsphericity, and surface irregularity and the prediction of bidirectional reflectance rather than merely fitting it empirically.

Note added in proof. *Ackerman and Toon* [1981] have calculated single scattering from atmospheric ammonium sulfate particles containing soot and have shown that the absorption is indeed enhanced by putting the soot particles inside the transparent sulfate particles. To reduce the aerosol single-scattering albedo from 1.0 to 0.85 required 10–20% soot (by volume) if the soot was present as separate particles but only 5% if the soot was located inside the sulfate particles. Similar results would be obtained for soot particles embedded in ice grains, as was speculated in section H1 above.

Acknowledgments. I thank Warren Wiscombe for considerable advice and discussion, especially for help with the zenith angle dependence of albedo. Craig Bohren and Jeff Dozier also made many helpful suggestions. This work is supported by NSF grant ATM-80-24641, and the computations were done at the National Center for Atmospheric Research. The first draft of this paper was presented as an invited review at the Joint U.S.-Canadian Workshop on the Properties of Snow, April 1981 (sponsored by CRREL and Montana State University).

References

Ackerman, T. P., and O. B. Toon, Absorption of visible radiation in atmosphere containing mixtures of absorbing and nonabsorbing particles, *Appl. Opt., 20*, 3661–3668, 1981.

Ambach, W., Untersuchungen zum Energieumsatz in der Ablationszone des Grönländischen Inlandeises, in *Expedition Glaciologique Internationale au Groenland*, vol. 4, pp. 76–78, Bianco Lunos, Copenhagen, 1963.

Ambach, W., and H. L. Habicht, Untersuchung der Extinktionseigenschaften des Gletschereises und Schnees, *Arch. Meteorol. Geophys. Bioklimatol., Ser. B, 11*, 512–532, 1962.

Barkstrom, B. R., Some effects of multiple scattering on the distribution of solar radiation in snow and ice, *J. Glaciol., 11*, 357–368, 1972.

Barkstrom, B. R., and C. W. Querfeld, Concerning the effect of anisotropic scattering and finite depth on the distribution of solar radiation in snow, *J. Glaciol., 14*, 107–124, 1975.

Bergen, J. D., A possible relation between grain size, density, and light attenuation in natural snow cover, *J. Glaciol., 9*, 154–156, 1970.

Bergen, J. D., The relation of snow transparency to density and air permeability in a natural snow cover, *J. Geophys. Res., 76*, 7385–7388, 1971.

Bergen, J. D. A possible relation of albedo to the density and grain size of natural snow cover, *Water Resourc. Res., 11* 745–746, 1975.

Berger, R. H., Snowpack optical properties in the infrared, *CRREL Rep. 79-11*, U. S. Army Cold Reg. Res. and Eng. Lab., Hanover, N. H.,1979. (Available as NTIS AD-A 071 004/6GA from the Natl., Tech. Inf. Serv., Springfield, Va.)

Blevin, W. R., and W. J. Brown, Effect of particle separation on the reflectance of semi-infinite diffusers, *J. Opt. Soc. Am., 51*, 129–134, 1961.

Bohren, C. F., and B. R. Barkstrom, Theory of the optical properties of snow, *J. Geophys. Res., 79*, 4527–4535, 1974.

Bohren, C. F., and R. L. Beschta, Snowpack albedo and snow density, *Cold Reg. Sci. Technol., 1*, 47–50, 1979.

Bolsenga, S. J., Spectral reflectances of freshwater ice and snow from 340 through 1100 nm, Ph.D. thesis, Univ. of Mich., Ann Arbor, 1981.

Bryazgin, N., and A. Koptev, Spectral albedo of snow-ice cover (in Russian), *Probl. Arktiki Antarkt., 31*, 79–83, 1969. (*Probl. Arctic Antarct., Engl. Transl., 29-32*, 355–360, 1970.)

Carroll, J. J., and B. W. Fitch, Dependence of snow albedos on solar elevation and cloudiness at the south pole, *J. Geophys. Res., 86*, 5271–5276, 1981.

Chernigovskii, N. T., Radiational properties of the ice cover of the central Arctic (in Russian), *Tr. Arkt. Antarkt. Naucho Issled. Inst., 253*, 1963. (*Hydrometeorology of the Polar Regions*, English translation, Israel Program for Scientific Translations, Jerusalem, 1967.)

Choudhury, B. J., Radiative properties of snow for clear sky solar radiation, *Cold Reg. Sci. Technol., 4*, 103–120, 1981.

Choudhury, B. J., and A. T. C. Chang, Two-stream theory of reflectance of snow, *IEEE Trans. Geosci. Electron., GE-17*, 63–68, 1979*a*.

Choudhury, B. J., and A. T. C. Chang, The solar reflectance of a snow field, *Cold Reg. Sci. Technol., 1*, 121–128, 1979*b*.

Choudhury, B. J., and A. T. C. Chang, On the angular variation of solar reflectance of snow, *J. Geophys. Res., 86*, 465–472, 1981.

Diamond, M., and R. W. Gerdel, Radiation measurements on the Greenland Ice Cap, *U.S. Army Snow, Ice Permafrost Res. Estab., Res. Rep. 19*, U.S. Army Cold Reg. Res. and Eng. Lab., Hanover, N. H., 1956.

Dirmhirn, I., and F. D. Eaton, Some characteristics of the albedo of snow, *J. Appl. Meteorol., 14*, 375–379, 1975.

Dobbins, R. A., and G. S. Jizmagian, Optical scattering cross

sections for polydispersions of dielectric spheres, *J. Opt. Soc. Am.*, *56*, 1345–1350, 1966.

Dozier, J., S. R. Schneider, and D. F. McGinnis, Jr., Effect of grain size and snowpack water equivalence on visible and near-infrared satellite observations of snow, *Water Resour. Res.*, *17*, 1213–1221, 1981.

Dunkle, R. V., and J. T. Bevans, An approximate analysis of the solar reflectance and transmittance of a snow cover, *J. Meteorol.*, *13*, 212–216, 1956.

Gate, L. F., Light-scattering cross sections in dense colloidal suspensions of spherical particles, *J. Opt. Soc. Am.*, *63*, 312–317, 1973.

Gates, D. M., *Biophysical Ecology*, Springer-Verlag, New York, 1980.

Giddings, J. C., and E. R. LaChapelle, Diffusion theory applied to radiant energy distribution and albedo of snow, *J. Geophys. Res.*, *66*, 181–189, 1961.

Gow, A. J., and T. Williamson, Volcanic ash in the Antarctic ice sheet and its possible climatic implications, *Earth Planet. Sci. Lett.*, *13*, 210–218, 1971.

Grenfell, T. C., An infrared scanning photometer for field measurements of spectral albedo and irradiance under polar conditions, *J. Glaciol.*, *27*, in press, 1981.

Grenfell, T. C., and G. A. Maykut, The optical properties of ice and snow in the Arctic basin, *J. Glaciol.*, *18*, 445–463, 1977.

Grenfell, T. C., and D. K. Perovich, Radiation absorption coefficients of polycrystalline ice from 400 nm to 1400 nm, *J. Geophys. Res.*, *86*, 7447–7450, 1981.

Grenfell, T. C., D. K. Perovich, and J. A. Ogren, Spectral albedos of an alpine snowpack, *Cold Reg. Sci. Technol.*, *4*, 121–127, 1981.

Griggs, M., Emissivities of natural surfaces in the 8- to 14-micron spectral region, *J. Geophys. Res.*, *73*, 7545–7551, 1968.

Griggs, M., and W. A. Marggraf, Measurement of cloud reflectance properties and the atmospheric attenuation of solar and infrared energy, *Rep. AFCRL-68-0003*, Air Force Cambridge Res. Lab., Bedford, Mass., 1967.

Hansen, J. E., Radiative transfer by doubling very thin layers, *Astrophys. J.*, *155*, 565–573, 1969.

Hanson, K., Radiation measurements on the Antarctic snowfield: A preliminary report, *J. Geophys. Res.*, *65*, 935–946, 1960.

Havens, J. M., Meteorology and heat balance of the accumulation area, McGill Ice Cap, Axel Heiberg Island, *Res. Rep. Meteorol. 2*, McGill Univ., Montreal, Que., 1964.

Hobbs, P. V., L. F. Radke, M. W. Eltgroth, and D. A. Hegg, Airborne studies of the emissions from the volcanic eruptions of Mount St. Helens, *Science*, *211*, 816–818, 1981.

Holmgren, B., *Climate and Energy Exchange on a Subpolar Ice Cap in Summer*, part E, *Radiation Climate*, Meteorologiska Institutionen, Uppsala Universitet, Uppsala, Sweden, 1971.

Hubley, R. C., Measurements of diurnal variations in snow albedo on Lemon Creek Glacier, Alaska, *J. Glaciol.*, *2*, 560–563, 1955.

Joseph, J. H., W. J. Wiscombe, and J. A. Weinman, The delta-Eddington approximation for radiative flux transfer, *J. Atmos. Sci.*, *33*, 2452–2459, 1976.

Kondratiev, K. Ya., Z. F. Miranova, and A. N. Otto, Spectral albedo of natural surfaces, *Pure Appl. Geophys.*, *59*, 207–216, 1964.

Korff, H. C., J. J. Gailiun, and T. H. Vonder Haar, Radiation measurements over a snowfield at an elevated site, *Atmos. Sci. Pap. 221*, Colo. State Univ., Fort Collins, 1974. (Available as NTIS N74-31878/3GI from the Natl. Tech. Inf. Serv., Springfield, Va.)

Kuhn, M., and L. Siogas, Spectroscopic studies at McMurdo, South Pole and Siple stations during the austral summer 1977–78, *Antarct. J. U. S. 13*, 178–179, 1978.

LaChapelle, E. R., *Field Guide to Snow Crystals*, University of Washington Press, Seattle, 1969.

Langleben, M. P., Albedo measurements of an Arctic ice cover from high towers, *J. Glaciol.*, *7*, 289–297, 1968.

Langleben, M. P., Albedo of melting sea ice in the southern Beaufort Sea, *J. Glaciol.*, *10*, 101–104, 1971.

Leu, D. J., Visible and near-infrared reflectance of beach sands: A study on the spectral reflectance/grain size relationship, *Remote Sens. Environ.*, *6*, 169–182, 1977.

Liljequist, G. H., Energy exchange of an Antarctic snow field: Short-wave radiation (Maudheim 71°03'S, 10°56'W), in *Norwegian-British-Swedish Antarctic Expedition, 1949–52, Scientific Results*, vol. 2, part 1A, Norsk Polarinstitutt, Oslo, 1956.

Matson, M., and D. R. Wiesnet, New data base for climate studies, *Nature*, *289*, 451–456, 1981.

Maykut, G. A., and P. E. Church, Radiation climate of Barrow, Alaska, 1962–66, *J. Appl. Meteorol. 12*, 620–628, 1973.

Meador, W. E., and W. R. Weaver, Two-stream approximations to radiative transfer in planetary atmospheres: A unified description of existing methods and a new improvement, *J. Atmos. Sci.*, *37*, 630–643, 1980.

Mellor, M., Engineering properties of snow, *J. Glaciol.*, *19*, 15–66, 1977.

Middleton, W. E. K., and A. G. Mungall, The luminous directional reflectance of snow, *J. Opt. Soc. Am.*, *42*, 572–579, 1952.

Nicodemus, F. E., J. C. Richmond, J. J. Hsia, I. W. Ginsberg, and T. Limperis, Geometrical considerations and nomenclature for reflectance, *NBS Monogr. 160, U. S.*, 52 pp., 1977. (Available as SD Cat. No. C13.44:160, U. S. Govt. Print. Office, Washington, D. C.)

Nussenzveig, H. M., and W. J. Wiscombe, Efficiency factors in Mie scattering, *Phys. Rev. Lett.*, *45*, 1490–1494, 1980.

O'Brien, H. W., and G. Koh, Near-infrared reflectance of snow-covered substrates, *CRREL Rep. 188*, U. S. Army Cold Reg. Res. and Eng. Lab., Hanover, N. H., in press, 1981.

O'Brien, H. W., and R. H. Munis, Red and near-infrared spectral reflectance of snow, *CRREL Res. Rep. 332*, U. S. Army Cold Reg. Res. and Eng. Lab., Hanover, N. H., 1975 (Available as NTIS AD-A007 732/1GI, from the Natl. Tech. Inf. Service, Springfield, Va.)

O'Neill, A. D. J., and D. M. Gray, Solar radiation penetration through snow, *IAHS AISH Publ.*, *107*, 227–241, 1973.

Ott, W., Strahlungsextinktion in homogenen Schneeschichten- Laserexperimente und Theorie des Strahlungstransportes, Ph.D. thesis, Univ. of Innsbruck, Innsbruck, Austria, 1974.

Patterson, E. M., Measurements of the imaginary part of the refractive index between 300 and 700 nanometers for Mount St. Helens ash, *Science*, *211*, 836–838, 1981.

Pfeffer, T., The effect of crevassing on the radiative absorptance of a glacier surface (abstract), *Ann. Glaciol.*, *3*, in press, 1982.

Pollack, J. B., and J. N. Cuzzi, Scattering by nonspherical particles of size comparable to a wavelength: A new semi-empirical theory and its application to tropospheric aerosols, *J. Atmos. Sci.*, *37*, 868–881, 1980.

Pollack, J. B., O. B. Toon, and B. N. Khare, Optical properties of some terrestrial rocks and glasses, *Icarus*, *19*, 372–389, 1973.

Post, A., and E. R. LaChapelle, *Glacier Ice*, University of Washington Press, Seattle, 1971.

Rahn, K. A., Relative importances of North America and Eurasia as sources of Arctic aerosol, *Atmos. Environ.*, *15*, 1447–1455, 1981.

Roessler, D. M., and F. R. Faxvog, Optoacoustic measurement of optical absorption in acetylene smoke, *J. Opt. Soc. Am.*, *69*, 1699–1704, 1979.

Rosen, H., T. Novakov, and B. A. Bodhaine, Soot in the Arctic, *Atmos. Environ.*, *15*, 1371–1374, 1981.

Roulet, R. R., G. A. Maykut, and T. C. Grenfell, Spectrophotometers for the measurement of light in polar ice and snow, *Appl. Opt.*, *13*, 1652–1658, 1974.

Rusin, N. P., *Meteorological and Radiational Regime of Antarctica* (in Russian), Gidrometeorologicheskoye Izdatel'stvo, Leningrad, 1961. (English translation, Israel Program for Scientific Translations, Jerusalem, 1964.)

Sagan, C., and J. B. Pollack, Anisotropic nonconservative scattering and the clouds of Venus, *J. Geophys. Res.*, *72*, 469–477, 1967.

Salomonson, V. V., and W. E. Marlatt, Anisotropic solar reflectance over white sand, snow, and stratus clouds, *Atmos. Sci. Pap. 120*, Colo. State Univ., Fort Collins, 1968*a*.

Salomonson, V. V., and W. E. Marlatt, Anisotropic solar reflectance over white sand, snow and stratus clouds, *J. Appl. Meteorol.*, *7*, 475–483, 1968*b*.

Sauberer, F., Die spektrale Strahlungsdurchlässigkeit des Eises, *Wetter Leben*, *2*, 193–197, 1950.

Schaff, J. W., and D. Williams, Optical constants of ice in the infrared, *J. Opt. Soc. Am.*, *63*, 726–732, 1973.

Schlatter, T. W., The local surface energy balance and subsurface temperature regime in Antarctica, *J. Appl. Meteorol.*, *11*, 1048–1062, 1972.

Schwerdtfeger, P., Absorption, scattering and extinction of light in ice and snow, *Nature, 222,* 378–379, 1969.

Schwerdtfeger, P., and G. E. Weller, Radiative heat transfer processes in snow and ice, in *Meteorological Studies at Plateau Station, Antarctica, Antarct. Res. Ser.*, vol. 25, edited by J. A. Businger, pp. 35–39, AGU, Washington, D. C., 1977.

Schwerdtfeger, W., The climate of the Antarctic, in *World Survey of Climatology*, vol. 14, edited by S. Orvig, pp. 253–355, Elsevier, New York, 1970.

Siegel, R., and J. R. Howell, *Thermal Radiation Heat Transfer*, McGraw-Hill, New York, 1972.

Stamnes, K., and R. A. Swanson, A new look at the discrete ordinates method for radiative transfer calculations in anisotropically scattering atmospheres, *J. Atmos. Sci., 38,* 387–399, 1981.

Stephenson, P. J., Some considerations of snow metamorphism in the Antarctic ice sheet in the light of ice crystal studies, in *Physics of Snow and Ice*, pp. 725–740, Bunyeido, Sapporo, Japan, 1967.

Stowe, L. L., H. Jacobowitz, and V. R. Taylor, Reflectance characteristics of earth and cloud surfaces as measured by the ERB scanning channels on the Nimbus-7 satellite, in *International Radiation Symposium Volume of Extended Abstracts*, pp. 430–432, Colorado State University, Fort Collins, 1980.

Sydor, M., J. A. Sorensen, and V. Shuter, Remote sensing of snow albedo for determination of dustfall, *Appl. Opt., 18,* 3574–3578, 1979.

Valovcin, F. R., Spectral radiance of snow and clouds in the near infrared spectral region, *Rep. AFGL-TR-78-0289*, Air Force Geophys. Lab., Hanscom Air Force Base, Bedford, Mass., 1978.

Warren, S. G., and W. J. Wiscombe, A model for the spectral albedo of snow, II, Snow containing atmospheric aerosols, *J. Atmos. Sci., 37,* 2734–2745, 1980.

Warren, S. G., and W. J. Wiscombe, Comment on "Radiative properties of snow for clear sky solar radiation," *Cold Reg. Sci. Technol., 5,* in press, 1981.

Weller, G. E., Heat-energy transfer through a four-layer system: Air, snow, sea ice, seawater, *J. Geophys. Res., 73,* 1209–1220, 1968.

Weller, G. E., Radiation diffusion in Antarctic ice media, *Nature, 221,* 355–356, 1969.

Wendler, G., and G. Weller, A heat-balance study on McCall Glacier, Brooks Range, Alaska: A contribution to the international Hydrological Decade, *J. Glaciol., 13,* 13–26, 1974.

Wendling, P., R. Wendling, and H. K. Weickmann, Scattering of solar radiation by hexagonal ice crystals, *Appl. Opt., 18,* 2663–2671, 1979.

Wiscombe, W. J., The delta-M method: Rapid yet accurate radiative flux calculations for strongly asymmetric phase functions, *J. Atmos. Sci., 34,* 1408–1422, 1977.

Wiscombe, W. J., Improved Mie scattering algorithms, *Appl. Opt., 19,* 1505–1509, 1980.

Wiscombe, W. J., and G. W. Grams, The backscattered fraction in two-stream approximations, *J. Atmos. Sci., 33,* 2440–2451, 1976.

Wiscombe, W. J., and S. G. Warren, A model for the spectral albedo of snow, I, Pure snow, *J. Atmos. Sci., 37,* 2712–2733, 1980*a*.

Wiscombe, W. J., and S. G. Warren, Solar and infrared radiation calculations for the Antarctic Plateau using a spectrally-detailed snow reflectance model, in *International Radiation Symposium Volume of Extended Abstracts*, pp. 380–382, Colorado State University, Fort Collins, 1980*b*.

Woronicz, R., The U. S. Air Force snow cover charts, *Glaciol. Data, 11,* 63–69, 1981. (Available from World Data Center-A for Glaciology, University of Colorado. Boulder.)

Zdunkowski, W. G., R. M. Welch, and G. Korb, An investigation of the structure of typical two-stream-methods for the calculation of solar fluxes and heating rates in clouds, *Beitr Phys. Atmos., 53,* 147–166, 1980.

(Received April 10, 1981;
accepted September 28, 1981.)